eIF4A is stimulated by the pre-initiation complex and enhances recruitment of mRNAs regardless of structural complexity

Paul Yourik[1], Colin Echeverría Aitken[1], Fujun Zhou[1], Neha Gupta[1,2], Alan G. Hinnebusch[2,3], Jon R. Lorsch[1,3]

[1]Laboratory on the Mechanism and Regulation of Protein Synthesis, Eunice Kennedy Shriver National Institute of Child Health and Development, National Institutes of Health, Bethesda, MD 20892

[2]Laboratory of Gene Regulation and Development, Eunice Kennedy Shriver National Institute of Child Health and Human Development, National Institutes of Health, Bethesda, MD 20892, USA

[3]Corresponding Author

ABSTRACT

eIF4A is a DEAD-box RNA-dependent ATPase thought to unwind RNA secondary structure in the 5'-untranslated regions (UTRs) of mRNAs to promote their recruitment to the eukaryotic translation pre-initiation complex (PIC). We show that the PIC stimulates the ATPase of eIF4A, indicating that the factor acts in association with initiating ribosomal complexes rather than exclusively on isolated mRNAs. ATP hydrolysis by eIF4A accelerates the rate of recruitment for all mRNAs tested, regardless of their degree of secondary structure, indicating that the factor plays important roles beyond unwinding mRNA structure. Structures in the 5'-UTR and 3' of the start codon synergistically inhibit mRNA recruitment, in a manner relieved by eIF4A, suggesting that the factor resolves global mRNA structure rather than just secondary structures in the 5'-UTR. We suggest that eIF4A breaks the many weak interactions formed within an mRNA that occlude the 5'-UTR and facilitates engagement of the 5'-UTR with the PIC.

INTRODUCTION

The goal of translation initiation is to assemble the ribosomal initiation complex containing the methionyl initiator tRNA (Met-tRNAi) at the translation start site on an mRNA. The process begins when the small (40S) subunit of the ribosome binds eIF1, eIF1A, eIF2, GTP, Met-tRNA$_i$, eIF3, and eIF5, to assemble the 43S PIC (Dever et al., 2016). eIF1 and eIF1A bind near the P site and in the A site of the 40S subunit, respectively, and promote binding of the ternary complex (TC) comprising eIF2, GTP, and Met-tRNA$_i$. eIF5 is the GTPase-activating protein (GAP) for eIF2 and promotes GTP hydrolysis (Das et al., 1997, 2001; Paulin et al., 2001); however, irreversible release of the inorganic phosphate is inhibited at this stage of the pathway (Algire et al., 2005). The heteromultimeric factor eIF3 has multiple

interactions with the PIC and is involved in nearly every step of translation initiation (Aitken and Lorsch, 2012; Valásek, 2012).

The 43S PIC is assembled in an "open" conformation (Fekete et al., 2007; Llacer et al., 2015; Maag et al., 2005, 2006; Passmore et al., 2007; Pestova et al., 1998) that can bind an mRNA in a process called mRNA recruitment. eIF3 and a set of mRNA recruitment factors – eIF4A, eIF4E, eIF4G, and eIF4B – facilitate this step (Mitchell et al., 2011). After initial mRNA loading, the PIC remains in an open conformation and scans the 5'- untranslated region (UTR) of the mRNA for the start codon, usually an AUG (Hinnebusch, 2014). Recognition of the start codon by the $tRNA_i$ triggers a series of key steps – eviction of eIF1, movement of the C-terminal tail of eIF1A out of the P site, and subsequent release of the previously-hydrolyzed inorganic phosphate by eIF2 – ultimately shifting the PIC from an "open" to a "closed" conformation (Dever et al., 2016; Hussain et al., 2014; Llacer et al., 2015). The 48S PIC thus formed is committed to the selected start codon and joining with the large (60S) subunit of the ribosome to form the final 80S initiation complex (Acker et al., 2009; Dever et al., 2016).

Whereas a combination of genetic, biochemical, and structural approaches have illuminated the molecular details of PIC formation and start-codon selection, the intermediate events of mRNA recruitment remain poorly understood (Aitken and Lorsch, 2012). We recently demonstrated that the absence of either eIF4A, eIF4B, eIF3, or eIF4G together with eIF4E, greatly reduces the extent, the rate or both for mRNA recruitment to the PIC in a *S. cerevisiae in vitro* reconstituted translation initiation system (Mitchell et al., 2010). Structural and biochemical work indicates that eIF3 binds on the solvent side of the 40S but its five core subunits have multiple interactions with other components of the PIC including distinct interactions with the mRNA near the entry and exit channels of the ribosome (Aitken et al., 2016; Llacer et al., 2015). Also, yeast eIF4B binds directly to the 40S ribosomal subunit, modulates the conformation of the ribosome near the mRNA entry channel (Walker et al., 2013), and has a functional interaction with eIF4A (Andreou and Klostermeier, 2014; Harms et al., 2014; Park et al., 2013; Walker et al., 2013). In contrast, eIF4A has not been shown to bind stably to the PIC but forms a heterotrimeric complex with eIF4G and eIF4E, collectively referred to as eIF4F, which interacts with the mRNA.

mRNA can form stable secondary structures via local base-pairing of complementary sequences but also has a natural tendency to form global structures, created by a combination of entangled or compacted conformations inherent to polymers longer than their persistence lengths (Chen et al., 2012) and the sum of many, possibly dynamic, individual base-pairing and other interactions between both neighboring and distant parts of the molecule (Halder and Bhattacharyya, 2013). Hairpin structures in the 5'-UTR are generally inhibitory to translation initiation and the prevailing

model of mRNA recruitment suggests that eIF4A – localized to the 5'-end via the eIF4G–eIF4E–5'-m^7G-cap chain of interactions – unwinds these hairpins to allow PIC attachment (Merrick, 2015; Pelletier and Sonenberg, 1985; Ray et al., 1985; Svitkin et al., 2001; Yoder-Hill et al., 1993).

eIF4A is a DEAD-box ATP-dependent RNA helicase (Andreou and Klostermeier, 2013a; Linder et al., 1989; Schreier et al., 1977). It cooperatively binds RNA and ATP with no apparent RNA sequence specificity, and is thought to disrupt structures by local strand separation, possibly due to bending of the RNA duplex (Henn et al., 2012; Linder and Jankowsky, 2011). Subsequent ATP hydrolysis causes a decrease in affinity of eIF4A for the mRNA, thus recycling eIF4A from an eIF4A•ATP•RNA ternary complex (Andreou and Klostermeier, 2013a; Jankowsky, 2011; Liu et al., 2008; Lorsch and Herschlag, 1998a, 1998b). Several studies demonstrated that eIF4A is able to disrupt short RNA duplexes (Rajagopal et al., 2012; Ray et al., 1985; Rogers et al., 1999) and more recent work suggests that eIF4A can unwind a large hairpin when the RNA is stretched between two tethers (Garcia-Garcia et al., 2015). Also, sensitivity to inhibition of translation by a dominant negative mutant of eIF4A is correlated with the degree of secondary structure in the 5'-UTR, supporting a role for eIF4A in removing structures from the 5'-end of mRNAs (Svitkin et al., 2001).

Nonetheless, eIF4A is a notoriously slow enzyme (Garcia-Garcia et al., 2015; Lorsch and Herschlag, 1998b; Rajagopal et al., 2012; Rogers et al., 1999) and it is difficult to envision how it supports *in vivo* rates of translation initiation in the regime of ~10 min^{-1} (Palmiter, 1975). In fact, several more potent helicases appear to promote translation by resolving stable structural elements (Parsyan et al., 2011), raising the possibility that eIF4A instead performs a distinct role during initiation on all mRNAs (Gao et al., 2016). A study employing ribosome profiling to compare the *in vivo* effects of inactivating eIF4A versus Ded1p – a considerably more robust DEAD-box RNA helicase – demonstrated that translation of many mRNAs with 5'-UTRs possessing high degrees of structure is highly dependent on Ded1 but relatively few mRNAs are similarly hyper-dependent on eIF4A, despite comparable requirements for the two helicases in maintaining global translation initiation. Consistent with this, analysis of reporter mRNAs harboring inhibitory hairpin structures indicated that yeast eIF4A is either ineffective or dispensable in the presence of Ded1 in resolving stable, local secondary structures in the 5'-UTR (Sen et al., 2015). In a separate study, minor decreases in the normally high cellular levels of eIF4A also resulted in depressed global rates of translation (Firczuk et al., 2013), providing additional evidence that eIF4A may be important for translation of all mRNAs and must be present in excess of other components of the translational apparatus. Consistent with the idea that it acts generally rather than by disrupting specific secondary structures in 5'-UTRs, eIF4A has been shown to promote translation of an mRNA possessing a short (8 nucleotide (nt)) 5'-UTR (Blum et al., 1992) and a viral mRNA with a low degree of structure in its

5'-UTR (Altman et al., 1990), and to stimulate 48S formation on mRNAs with little secondary structure in their 5'-UTRs (Pestova and Kolupaeva, 2002). How the helicase and ATPase activities of eIF4A, alone or as a part of eIF4F, contribute to its role in promoting initiation on diverse mRNAs remains unclear.

Here – using an *in vitro* translation initiation system reconstituted from purified *S. cerevisiae* components – we examined the role of eIF4A and eIF4F in mRNA recruitment to the PIC. We monitored the kinetics of eIF4A ATPase activity in the context of mRNA recruitment and asked how that activity is utilized for the recruitment of mRNAs possessing various degrees of structure, ranging from the natural (structured) *RPL41A* mRNA to short model mRNAs comprised mostly of CAA repeats expected to lack significant structure (hereafter called "unstructured") (Sobczak et al., 2010; Zuker, 2003) beyond fluctuations in polymer conformation or transient interactions (Chen et al., 2012). We show that the PIC stimulates the ATPase activity of eIF4A both on its own and as a component of eIF4F. We further show that eIF4A increases the rate of recruitment of all mRNAs tested, ranging from the natural *RPL41A* mRNA to short unstructured messages. Structures in the 5'-UTR and on the 3' side of the start codon synergistically inhibit mRNA recruitment in a manner relieved by eIF4A. We propose that eIF4A, alone or as a part of eIF4F, facilitates mRNA recruitment and PIC attachment by relaxing global mRNA structure rather than resolving specific secondary structures in the 5'-UTR. In addition, our data indicate the factor engages with the PIC, consistent with the possibility that it facilitates loading of mRNAs into the 40S subunit's entry channel by remodeling the PIC itself or by funneling the message directly onto the ribosome.

RESULTS

ATP hydrolysis by eIF4A is required for recruitment of mRNAs, regardless of their degree of structure

To better understand how eIF4A-catalyzed ATP hydrolysis is related to the removal of RNA structure and mRNA recruitment, we compared the kinetics of recruitment of the natural mRNA *RPL41A* (possessing structural complexity throughout its length) with a 50 (nt) model mRNA made up of CAA repeats and an AUG codon at positions 24-26 (CAA 50-mer) (Aitken et al., 2016). The latter mRNA is expected to have little, if any, secondary or tertiary structure (Sobczak et al., 2010; Zuker, 2003).

mRNA recruitment experiments were performed as described previously, using an *in vitro*-reconstituted *S. cerevisiae* translation initiation system (Mitchell et al., 2010; Walker et al., 2013). Briefly, PICs containing 40S, TC, eIF1, eIF1A, eIF5, and eIF3 were formed in the presence of saturating levels of eIFs 4A, 4B, 4E, and 4G (see "30 nM PIC" in Methods). Reactions were initiated by simultaneous addition of ATP and an mRNA labeled with a [^{32}P]-7-

methylguanosine (m^7G) cap, enabling mRNA recruitment to the PICs and formation of 48S complexes. Reaction timepoints were acquired by mixing an aliquot with a 25-fold excess of a non-radioactive ("cold") capped mRNA identical to the labeled one in the reaction, effectively stopping further recruitment of radiolabeled mRNA. The rate of dissociation of recruited mRNAs from the PIC in the presence of the cold chase mRNA was negligible for all mRNAs in the study (data not shown). Free mRNA and 48S complexes were resolved via gel electrophoresis on a native 4% THEM polyacrylamide gel (Acker et al., 2007; Mitchell et al., 2010) (see Materials and Methods).

We first compared the kinetics of recruitment for *RPL41A* with CAA 50-mer in the presence and absence of ATP (Figure 1). In the presence of saturating ATP, the rate of recruitment of *RPL41A* was 0.74 ± 0.01 min^{-1} with an endpoint in excess of 90%. In contrast, in the presence of ADP, and in reactions lacking either nucleotide or eIF4A, less than 20% of *RPL41A* mRNA was recruited after 6 hours, indicating a dramatically lower rate that could not be measured accurately due to the low reaction endpoint (Figure 1A,C). The CAA 50-mer was recruited in the absence of eIF4A and ATP at rates of about 0.90 min^{-1}, likely due to lack of significant structure, reaching endpoints around 80%. Surprisingly, the addition of eIF4A and ATP stimulated the rate of recruitment of the CAA 50-mer by more than 4-fold (4.0 ± 0.6 min^{-1}) and yielded an endpoint of 90% (Figure 1B,C).

To determine whether ATP hydrolysis is required for the stimulation we observed, we next measured the rate of recruitment with the non-hydrolyzable ATP analogs ADPCP and ADPNP, as well as with the slowly-hydrolyzable analog ATP-γ-S (Peck and Herschlag, 2003). Neither ADPCP nor ADPNP supported stimulation of the recruitment of either mRNA by eIF4A, producing rates that were comparable to the observed rates measured in the absence of nucleotide or eIF4A (Figure 1; compare grey and blue curves to red and purple). In the presence of ATP-γ-S, recruitment of *RPL41A* and CAA 50-mer was 39-fold (0.019 ± 0.001 min^{-1}) and nearly 2-fold (2.3 ± 0.2 min^{-1}) slower, respectively, than in the presence of ATP; however, both mRNAs achieved endpoints of approximately 80%, consistent with previous observations that eIF4A is capable of utilizing ATP-γ-S (Peck and Herschlag, 2003). Taken together, these results suggest that ATP hydrolysis by eIF4A is required to stimulate the recruitment of mRNAs to the PIC regardless of their degree of structure.

The ATPase activities of eIF4A and eIF4F are increased by the PIC

We next asked if the presence of the PIC might influence the activity of eIF4A or eIF4F. We monitored the ATPase activity of eIF4A in the *in vitro* reconstituted translation initiation system using an enzyme-coupled ATPase assay

in which pyruvate kinase and lactate dehydrogenase are used to regenerate ATP from ADP and, in the process, oxidize NADH to NAD^+, producing a change in absorbance at 340 nm (Bradley and De La Cruz, 2012; Kiianitsa et al., 2003); (Figure 2 – figure supplement 1A; see Materials and Methods). Reactions with varying concentrations of mRNA were assembled in a 384-well plate and initiated by addition of saturating ATP (5 mM). NADH absorbance at 340 nm was recorded every 20 seconds using a microplate reader. By titrating mRNA, we determined the maximal velocity of ATP hydrolysis (V_{max}), as well as the concentration of mRNA needed to achieve the half-maximal velocity (K_m^{RNA}). For eIF4A alone (5 μM) the V_{max} was 2.4 ± 0.2 μM/min (or a k_{cat} of 0.48 ± 0.04 min^{-1}) (Figure 2A; Figure 2 – figure supplement 1B), comparable to a previous measurement of k_{cat} of 0.20 ± 0.05 min^{-1} (Rajagopal et al., 2012). Also, congruent with previous findings (Hilbert et al., 2011; Oberer et al., 2005; Rajagopal et al., 2012), the addition of co-purified full length eIF4G1 and eIF4E (eIF4G•4E) to eIF4A, forming the eIF4F complex, resulted in a 6.5-fold increase in the V_{max} at saturating mRNA levels (Figure 2A; compare "4A alone" to "4A•4G•4E alone").

The addition of the PIC to these reactions (See "0.5 μM PIC" in Methods) increased the observed V_{max} an additional 3-fold over the V_{max} with eIF4F alone (Figure 2A; compare "4A•4G•4E alone" to "+"). Leaving out the 40S subunit resulted in a 2-fold decrease of V_{max} as compared to the value observed in the presence of an intact PIC (Figure 2A), suggesting that the 40S, alone or in association with one or more components of the PIC stimulates the ATPase activity. We observed similar values for K_m^{RNA} in the presence of a complete PIC (260 ± 40 μM) and when all components except the 40S were present (270 ± 70 μM). In contrast, the K_m^{RNA} with eIF4A and eIF4F alone were 80 ± 10 μM and 100 ± 10 μM, respectively (Figure 2A; Figure 2 – Supplement 1B). Because values of V_{max} are, by definition, obtained at saturating concentrations of mRNA (Figure 2A), the stimulation observed by the PIC is not attributable to rRNA or $tRNA_i$.

Because the 5'-cap promotes mRNA recruitment (Kumar et al., 2016; Mitchell et al., 2010), we also measured the V_{max} and K_m^{RNA} with uncapped *RPL41A*. In the presence of the PIC, the V_{max} was comparable and the K_m^{RNA} was approximately 2-fold lower than the values measured with capped *RPL41A*. For eIF4F alone, in the absence of the PIC, congruent with previous findings (Rajagopal et al., 2012), the V_{max} (21.3 ± 0.1 μM/min) and the K_m^{RNA} (150 ± 24 μM) were both modestly higher with uncapped RPL41A than with capped. The absence of a cap on the mRNA did not affect the enhancement of the maximal rate of ATP hydrolysis by the PIC at saturating concentrations of mRNA (Figure 2 – figure supplement 1C).

The rate of eIF4A-catalyzed ATP hydrolysis saturates at levels of eIF4A in excess of the PIC

In vivo eIF4A is in excess of all other components of the translational machinery and the rate of translation is sensitive to minor changes in eIF4A concentration (Firczuk et al., 2013; von der Haar and McCarthy, 2002). *In vitro,* the maximal rate of mRNA recruitment is observed when eIF4A is in excess of the PIC, mRNA, and other initiation factors (Mitchell et al., 2010; Walker et al., 2013). To determine how the eIF4A:PIC ratio affects the stimulation of eIF4A by the PIC, we titrated eIF4A in the presence of saturating capped *RPL41A* mRNA and ATP. The rate of ATP hydrolysis observed in the presence of the PIC was divided by the rate observed with the same concentration of eIF4A alone (i.e. normalized) (Figure 2B). Titrating eIF4A to increase the eIF4A:PIC ratio, resulted in a larger enhancement of the normalized rate of ATP hydrolysis, plateauing at a concentration of eIF4A in 10-fold excess of the PIC (5 μM eIF4A), consistent with the requirement of excess eIF4A for mRNA recruitment, both *in vivo* and *in vitro*. It is possible that this concentration of eIF4A is necessary to saturate the PIC due either to a relatively weak interaction or to the presence of multiple binding sites for the factor on the mRNA and/or the PIC. The degree of ATPase stimulation by the PIC modestly decreased when eIF4A was in excess over the PIC by 24-fold (12 μM eIF4A) possibly because all available PICs were saturated by eIF4A (Figure 2B) and could not provide as much of a rate increase when normalized to the rate of eIF4A alone at that concentration.

The PIC and eIF4G•4E stimulate eIF4A via distinct mechanisms

Having observed that the PIC increases the rate of eIF4A-catalyzed ATP hydrolysis at saturating levels of ATP and mRNA, we next investigated the effects of the PIC and eIF4G•4E on the ATP-dependence of the reaction. As before, we measured ATPase activity in the presence and absence of the PIC but here performed experiments with saturating capped *RPL41A* mRNA (0.5 μM) and instead varied the ATP concentration to determine the maximal velocity of ATP hydrolysis at saturating ATP levels (V_{max}) and the concentration of ATP required to achieve half-maximal velocity (K_m^{ATP}) (Figure 2C). In the absence of the PIC and other initiation factors, eIF4A alone hydrolyzed ATP at a maximal velocity of 2.9 ± 0.4 μM/min and had a K_m^{ATP} of 2500 ± 400 μM. The presence of eIF4G•4E – forming eIF4F – resulted in a 4-fold increase in the V_{max} (11.9 ± 0.6 μM/min) and a 10-fold decrease in K_m^{ATP} (250 ± 10 μM). Adding the PIC to eIF4F increased the V_{max} an additional 4-fold but had no significant impact on K_m^{ATP} (Figure 2C, "4A alone," "4A•4G•4E alone," "+"). Omitting the 40S subunits from reactions containing eIF4F and all other PIC components decreased the V_{max} by a factor of 2 underscoring the importance of the 40S subunit in promoting ATPase activity (Figure 2C, compare "-40S" to "+"). The absence of the 40S subunit also resulted in a 2-fold decrease in the

K_m^{ATP}. In contrast, adding only the 40S and TC to eIF4F did not provide a significant increase in the rate of ATPase as compared with eIF4F alone (Figure 2 – Figure Supplement 1D, "TC, 40S, 4A•4G•4E"), suggesting that the 40S is not able to directly stimulate eIF4F and requires other PIC components. Also, the omission of eIF4A from a reaction containing all other components resulted in ≥ 67-fold decrease in the rate of ATPase (to the limit of detection of the assay), ruling out any significant ATPase contamination in either the PIC components or other initiation factors (Figure 2C, "-4A").

We next asked if the PIC could stimulate eIF4A ATPase directly, in the absence of eIF4G•4E. Addition of the PIC to eIF4A, in the absence of eIF4G•4E, resulted in a 6-fold increase in V_{max} over eIF4A alone (Figure 2C, "4A alone" vs. "-4G, -4E") and a K_m^{ATP} that was ~1.5-fold lower than that with eIF4A alone. eIF4G is thought to juxtapose the two eIF4A RecA-like domains to enhance ATP binding and catalysis (Hilbert et al., 2011; Oberer et al., 2005; Schütz et al., 2008), potentially explaining eIF4F's significantly lower K_m^{ATP} than that of eIF4A alone. Our findings that eIF4G•4E increased the V_{max} by 4-fold and decreased the K_m^{ATP} by 10-fold, as compared to eIF4A alone (Figure 2C "4A alone", "4A•4G•4E alone"), whereas the PIC increased the V_{max} with only a small decrease in the K_m^{ATP} (Figure 2C "4A alone", "-4G•4E") may be due to distinct mechanisms of eIF4A stimulation. Taken together, our data suggest that the PIC enhances ATP hydrolysis without a major effect on ATP binding, while eIF4G•4E stimulates both ATP binding and hydrolysis.

eIF3 and other components of the PIC are required for full stimulation of eIF4A

To further dissect the functional interactions among eIF4A, eIF4G•4E, and the PIC, we next measured V_{max} and K_m^{ATP} in the absence of each of the PIC components. Leaving out $tRNA_i$ or eIF2 decreased the V_{max} by ~2-fold – similar to the reduction observed in the absence of 40S subunits – and also conferred a 1.5-fold reduction in K_m^{ATP} as compared to when all components were present (Figure 2C; compare "+" to "-2", and "-$tRNA_i$"). The absence of eIF1 or eIF1A, which both stimulate binding of the TC to the 40S subunit (Hinnebusch, 2014), also resulted in ~1.3-fold reductions in V_{max}. Leaving out eIF3 decreased the V_{max} by approximately 2.5-fold and K_m^{ATP} by approximately 2-fold. In contrast, eIF3 did not significantly influence V_{max} or K_m^{ATP} in the presence of eIF4F alone (Figure 2 – figure supplement 1D, compare "eIF4A•4G•4E alone" to "3, 4A•4G•4E"), indicating that its effect is exerted only in the presence of other PIC components. Taken together, the PIC stimulation of eIF4A that we observe depends on the presence of the

majority of PIC constituents. The changes in K_m^{ATP} could be due to conformational differences in eIF4A in the absence of PIC components or changes in the rate-limiting step for ATP hydrolysis (Fersht, 1999).

S. cerevisiae eIF3 is comprised of 5 core subunits and is involved in numerous steps of translation initiation, including mRNA recruitment. Previous reports demonstrated that yeast eIF3 is essential for mRNA recruitment both *in vitro* (Mitchell et al., 2010) and *in vivo* (Jivotovskaya et al., 2006), and that it stabilizes TC binding and promotes PIC interactions with the mRNA at both the mRNA entry and exit channels of the 40S subunit (Aitken et al., 2016). In particular, the eIF3 subunits g and i have been implicated in scanning and AUG recognition *in vivo* (Cuchalová et al., 2010) and are required for recruitment of *RPL41A* mRNA *in vitro* (Aitken et al., 2016; Valásek, 2012). Both subunits are thought to be located near the mRNA entry channel of the ribosome, at either the solvent or intersubunit face of the 40S subunit (Aylett et al., 2015; des Georges et al., 2015; Llacer et al., 2015). In the presence of PICs formed with the heterotrimer of eIF3 subunits a, b, and c – but lacking the g and i subunits – eIF4F had V_{max} and K_m^{ATP} values of 20 ± 2 μM/min and 170 ± 12 μM, respectively, which were similar to those observed in the absence of the entire eIF3 (Figure 2C, "-3" vs. "-3g, -3i"). Thus, although the heterotrimeric eIF3a,b,c subcomplex binds to the PIC under our experimental conditions (Aitken et al., 2016), it does not stimulate eIF4F's ATPase activity, indicating an important role for the eIF3 i and g subunits in this function.

Having found that the PIC can stimulate eIF4A ATPase activity in the absence of eIF4G•4E (Figure 2C), we next asked which PIC components are critical for this independent stimulatory mechanism. Eliminating the 40S subunit, eIF2, eIF3, or the g and i subunits of eIF3 in the absence of eIF4G•4E abrogated all stimulation of ATPase activity, yielding V_{max} values the same as observed with eIF4A alone (~3 μM/min^{-1}) (Figure 2D). The K_m^{ATP} values were also similar to the values observed with eIF4A alone or when just eIF4G•4E was missing from the PIC (~1600 μM, Figure 2D). Taken together, these data suggest that stimulation of the ATPase activity of eIF4A, in the absence of eIF4G•4E, requires multiple components of the PIC. In the presence of eIF4G•4E, the combined absence of the 40S subunit and either eIF2 or eIF3 yielded K_m^{ATP} and V_{max} values that were comparable to those obtained in the presence of the 40S subunit when only eIF2 or eIF3 were left out of the reaction, as well as to reactions in which just the 40S subunit was omitted (Figure 2D compare "-2, -40S" and "-3, -40S" to Figure 2C "-40S," "-2" and "-3"), suggesting that the stimulatory effects of eIF2, eIF3 and the 40S subunit are interdependent and largely reflect the 40S-bound conformations of the factors. It may be noteworthy, however, that the omission of eIF3 or its g and i subunits consistently has a slightly larger effect on the V_{max} of ATP hydrolysis in the presence of eIF4G•4E and other components of the PIC than does omission of the 40S subunit or eIF2 (Figure 2C, compare "-3" and "-3g, -3i" to "-

40S" and "-2"; Figure 2D, compare "-3, -40S" to "-2, -40S"). This observation suggests that eIF3 might provide a small amount of stimulation of eIF4F's ATPase in the absence of a fully assembled PIC, but in a manner that depends on one or more additional factors.

The PIC stimulates ATP hydrolysis by eIF4F in the presence of limiting amounts of either a structured natural mRNA or a short unstructured model mRNA

Our initial observation that eIF4A stimulates the recruitment of both the natural *RPL41A* mRNA and the unstructured CAA 50-mer model mRNA was made under conditions of limiting mRNA, whereas our experiments investigating the stimulation of eIF4A ATPase by the PIC and other initiation factors were performed at saturating mRNA levels and higher factor concentrations to ensure PIC formation even in the absence of multiple components. To confirm that the PIC stimulation of eIF4A's ATPase activity is maintained at limiting mRNA levels, we monitored ATP hydrolysis by eIF4A (in the context of the eIF4F complex) in the presence or absence of the PIC (30nM PIC, when present, the same conditions as in Figure 1), using limiting (15 nM) capped *RPL41A* or capped CAA 50-mer. As under saturating mRNA conditions, addition of the PIC increased the V_{max} approximately 4-fold in the presence of both the natural *RPL41A* and the unstructured CAA 50-mer mRNAs, as compared to eIF4F alone (Figure 2E). Thus, the PIC stimulates eIF4A activity under conditions where eIF4A promotes PIC recruitment of both native and unstructured model mRNAs. Also, the K_m^{ATP} was ~3-fold higher than observed with saturating mRNA and 0.5 μM PIC (compare Figure 2E and 2C, blue bars). Considering that eIF4A binds RNA and ATP cooperatively (Lorsch and Herschlag, 1998b), perhaps the mRNA was sub-saturating for eIF4A binding at the lower concentration (15 nM) employed in the current experiments (Figure 2E), which imposed a requirement for higher ATP concentrations to saturate ATP binding.

In contrast to the other PIC components, we did not observe an effect on the V_{max} of eIF4A ATPase by omitting eIF5. Similarly, leaving out eIF4B, in the presence or absence of the PIC, had no effect on V_{max} for ATP hydrolysis (Figure 2C, E; Figure 2 – figure supplement 1D). However, addition of eIF4B in the presence of either eIF4F alone or with eIF4F and the complete PIC, decreased the K_m^{ATP} by 1.5-fold and 2.5-fold, respectively, as compared to the corresponding condition in the absence of eIF4B (Figure 2C; Figure 2 – figure supplement 1D) consistent with the idea that eIF4B acts as a coupling factor or a co-factor for eIF4A (Andreou and Klostermeier, 2014; Mitchell et al., 2010; Özeş et al., 2011). Although eIF4B has no effect on the V_{max} for ATP hydrolysis in our system, the factor strongly stimulates mRNA recruitment to the PIC *in vitro* (Mitchell et al., 2010), demonstrating that it is active. It also reduces the $K_{1/2}$ for eIF4A in mRNA recruitment assays, indicating a functional coupling between the two factors exists in the *in*

vitro system (Walker et al., 2013). Therefore, the lack of an effect of eIF4B on the ATPase activity of eIF4A in the system does not appear to represent a functional inadequacy.

eIF4A relieves the inhibition of recruitment created by the global structures of mRNAs, rather than structures confined to the 5'-UTR

Our finding that eIF4A-dependent ATP hydrolysis increases the rate of recruitment of a natural mRNA as well as a short, unstructured 50 nucleotide model mRNA prompted us to investigate which features of an mRNA influence the efficiency of its recruitment to the PIC and the dependence on eIF4A. To this end, we created a library of *in vitro* transcribed and individually purified mRNAs spanning a range of structures and lengths. This library contains model mRNAs made almost entirely of CAA repeats, containing or lacking a 9 base pair (bp) hairpin in the 5'-UTR, and/or a natural *RPL41A* mRNA sequence downstream of the AUG in place of CAA repeats (Figure 3A; Supplementary Methods). We measured the recruitment kinetics for each mRNA as a function of eIF4A (as described above; see "mRNA Recruitment Assay" in Methods) and determined the maximal rate (k_{max}) and concentration of eIF4A required to achieve the half-maximal rate ($K_{1/2}^{eIF4A}$) (Figure 3 – figure supplement 1).

Using an eIF4A concentration determined to be at, or close to, saturation for all ten mRNAs (5 μM, as determined in Figure 3 – figure supplement 1), we observed recruitment endpoints between 85%-95% with all mRNAs tested (Figure 3B, black bars). In the absence of eIF4A, however, the extent of recruitment varied widely among the mRNAs. Less than 10% of *RPL41A* mRNA was recruited in reactions lacking eIF4A (Figure 3B, RNA 10, red bar), consistent with the low levels of *RPL41A* recruitment we observed in the absence of ATP (Figure 1A), with a k_{max} of 1.3 ± 0.1 min^{-1} (Figure 3C) and $K_{1/2}^{eIF4A}$ of 3.7 ± 1.0 μM (Figure 3 – figure supplement 1B,E). In the absence of eIF4A, time courses with *RPL41A* mRNA could not be accurately fit to a single-exponential kinetic model due to low reaction endpoints. However, comparison of estimated initial rates (no eIF4A, 0.22 ± 0.07 min^{-1}; saturating eIF4A, 41 ± 1 min^{-1}) of recruitment of *RPL41A* revealed that recruitment proceeds two orders of magnitude more rapidly in the presence of saturating levels of eIF4A versus in the absence of eIF4A (Figure 3D).

Consistent with our observation that the unstructured CAA 50-mer mRNA is efficiently recruited even in the absence of ATP, we observed 74 ± 1 % recruitment of this mRNA in the absence of eIF4A (Figure 3A-B, RNA 1, red bar). Nonetheless, the addition of saturating eIF4A increased the extent of recruitment to 87 ± 1 % (Figure 3A-B, RNA 1, black bar) consistent with our observation that the addition of ATP slightly elevates the extent of recruitment of this mRNA above the levels observed in the absence of ATP (Figure 1B). Beyond this modest stimulation of recruitment

extent, saturating eIF4A accelerated the rate of CAA 50-mer recruitment, yielding a k_{max} of 6.2 ± 1.0 min^{-1} (Figure 3C), a more than 7-fold increase (Figure 3D) as compared to the rate of CAA 50-mer recruitment in the absence of eIF4A (0.9 ± 0.1 min^{-1}). Relative to *RPL41A* mRNA, this acceleration is achieved at lower levels of eIF4A ($K_{1/2}^{eIF4A}$ of 0.70 ± 0.2 μM vs. 3.7 ± 1.0 μM with RPL41A; Figure 3 – figure supplement 1B,E).

To compare the CAA 50-mer with a longer mRNA, we increased the total mRNA length to 250 nucleotides (250-mer) by adding 200 nucleotides of CAA repeats downstream of the AUG (Figure 3A, RNA 2). In the absence of eIF4A, we observed 66 ± 10 % extent of recruitment, comparable to that seen for the CAA 50-mer in the absence of eIF4A (Figure 3B, red bars, RNA 1 vs. 2). The k_{max} was 3.3 ± 0.4 min^{-1}, approximately 2-fold lower than that for the CAA 50-mer, whereas the $K_{1/2}^{eIF4A}$ values were indistinguishable for the two mRNAs (Figure 3 – figure supplement 1E). Importantly, eIF4A strongly stimulated the rate of recruitment of this mRNA, in this case by 13-fold (Figure 3D). Similar results were obtained for two additional CAA-repeat 250-mers with the AUG situated 67 or 150 nucleotides from the 5'-end (Figure 3A, RNAs 3 and 4). These mRNAs had extents of recruitment of 60-70% in the absence of eIF4A, which increased to >90% in the presence of saturating eIF4A (Figure 3B, RNAs 3-4, red vs. black bars). Furthermore, the k_{max} for mRNA recruitment in the presence of eIF4A (Figure 3C, RNAs 3-4) were 22- and 7-fold greater than the observed rates in the absence of eIF4A (Figure 3D, RNAs 3-4). The k_{max} values and degree of stimulation by eIF4A varied by ≤2-fold among RNAs 1-4. The reason for these differences is not clear, but does not seem to correlate with overall mRNA length or number of nucleotides 5' or 3' to the AUG. Thus, all four unstructured CAA-repeat mRNAs that we studied can be recruited by the PIC at appreciable levels independently of eIF4A, but eIF4A stimulates their rates of recruitment by roughly an order of magnitude.

To probe the effects of defined, stable secondary structures on the functioning of eIF4A in mRNA recruitment, we examined 250-mer mRNAs comprising CAA repeats throughout the sequence except for a single 21-nt insertion predicted to form an 9 bp hairpin of -10 kcal/mol stability (Zuker, 2003), situated in the 5'-UTR either proximal or distal to the 5'-cap (Figure 3A, RNAs 5-6, Key; Supplementary Methods). Both cap-proximal and cap-distal insertion of this 21-nt sequence into the 5'-UTR of a luciferase reporter conferred strong inhibition of reporter mRNA translation in yeast cells (Sen et al., 2016). We confirmed the presence and location of the single hairpin in RNAs 5 and 6 and absence of significant secondary structure in RNA 4 by incubating RNAs 4-6 at 26°C with a 3'-5' RNA exonuclease, ExoT, specific for single-stranded RNA (Figure 3 – figure supplement 2); (Deutscher et al., 1984; Zeng and Cullen, 2004).

To our surprise, in the absence of eIF4A, neither the cap-proximal nor the cap-distal hairpins significantly influenced the extent of recruitment, achieving endpoints between 70% and 80%, comparable to the unstructured CAA 50-mer and 250-mer RNAs (Figure 3B, RNAs 5-6 vs. 1-4). The maximal rates in the presence of eIF4A for both hairpin-containing mRNAs (RNAs 5-6) were ~2-fold lower than for the CAA 250-mers lacking the hairpin (RNAs 1-4) but ~2-3-fold higher than the k_{max} for *RPL41A* (Figure 3C, RNAs 5-6 vs. 10). We could not accurately measure the $K_{1/2}^{eIF4A}$ for RNAs 5 and 6 but the lower limit was between 60-200 μM (Fersht, 1999). Saturating eIF4A stimulated the rate of recruitment for both cap-proximal and cap-distal hairpin mRNAs but, surprisingly, to a lesser degree than in the absence of the hairpin: between 3- and 4-fold as opposed to 7-fold for RNA 4 (Figure 3D). Thus, at odds with the expectation that stable structures in the 5'-UTR would impose strong obstacles to mRNA recruitment to the PIC, we found that addition of a cap-proximal or cap-distal hairpin in the 5'-UTR of an otherwise unstructured mRNA confers little or no inhibition of the extent of recruitment and only a modest reduction in the rate, in the presence or absence of eIF4A. Moreover, the observation that these hairpins in the 5'-UTR actually decrease the enhancement of the rate of mRNA recruitment provided by eIF4A relative to what we observed with the unstructured mRNA (Figure 3D, RNAs 5-6 vs. 4) is not readily consistent with the idea that the factor's predominant function is to unwind stable secondary structures in the 5'-UTRs of mRNAs. If this were the case, one might have expected larger rate enhancements for mRNAs with stable structures in their 5'-UTRs than for mRNAs containing little inherent structure, the opposite of what we actually observe. It is possible that eIF4A is not efficient at unwinding such stable structures, which results in a lower k_{max} and a lower degree of stimulation.

To probe further the effects of RNA structural complexity on mRNA recruitment and eIF4A function, we examined a chimeric mRNA comprising CAA-repeats in the 5'-UTR and the natural sequence (with associated structural complexity) from *RPL41A* 3' of the AUG start codon (Figure 3A, RNA 7). In the absence of eIF4A, this mRNA was recruited to the PIC with an observed rate of 0.06 ± 0.01 min^{-1}, which is significantly slower than for RNAs 1-6 (~0.2-0.9 min^{-1}), but faster than the rate for full-length *RPL41A* mRNA, which could not be determined due to its low endpoint of recruitment (Figure 3 – supplement 1B,E RNAs 1-6, 10 vs. 7). In contrast, in the presence of saturating eIF4A the k_{max} for RNA 7 was comparable to the k_{max} values observed with RNAs 2, 3, 5 and 6 and within 2-fold of the values for RNAs 1 and 4. Thus, addition of saturating eIF4A conferred a 60-fold increase in the rate of recruitment for RNA 7, which is a greater degree of stimulation than observed with RNAs 1-6 (Figure 3D), indicating that eIF4A can efficiently resolve inhibition of mRNA recruitment mediated by RNA sequences on the 3' side of the start codon that are not predicted to form stable secondary structures with the 5'-UTR (Zuker, 2003). In addition, the $K_{1/2}^{eIF4A}$ for RNA 7

was 1.8 ± 0.9 μM, approximately midway between the unstructured model mRNAs (RNAs 1-4; Figure 3 – supplement 1E; $K_{1/2}^{4A}$ values of 0.7-1.0 μM) and *RPL41A* (3.7 ± 1.0 μM), suggesting that structure on the 3' side of the start codon increases the concentration of eIF4A required to maximally stimulate recruitment.

The cap-proximal and cap-distal hairpins were strongly inhibitory to mRNA recruitment in the absence of eIF4A when inserted into the unstructured 5'-UTR of the chimeric mRNA harboring *RPL41A* sequence 3' of the AUG codon, conferring very low reaction endpoints (≤ 20%; Figure 3B, RNAs 8-9, red bars) and rates (Figure 3 – figure supplement 1E, $k_{obs}^{no\ eIF4A}$, RNAs 8-9). The presence of saturating eIF4A increased recruitment of both of these mRNAs to ~80% (Figure 3B, RNAs 8-9, black vs. red bars) and also increased their k_{max} values by approximately 10-fold (Figure 3D, RNAs 8-9); however, the rate stimulation by eIF4A was notably less than the 60-fold and ~190-fold increases observed for the chimeric mRNA lacking a hairpin (RNA 7) and native *RPL41A* (RNA 10), respectively (Figure 3D, RNAs 8-9 vs. 7,10). Consequently, the maximal rates achieved in the presence of eIF4A for mRNAs 8-9 remain well below those observed for mRNA 7 and *RPL41A* mRNA (Figure 3C, RNAs 8-9 vs. 7 and 10). Notably, the hairpin insertions conferred the predicted strong inhibition of PIC recruitment in the context of the chimeric mRNA containing native *RPL41A* sequences, but not in an otherwise unstructured mRNA.

Comparing k_{max} values for RNA 4 to RNAs 5-9 shows that the combined effects of structures in the 5'-UTR and 3' to the AUG (RNAs 8 and 9) is considerably more than the additive effects of either structural element alone (Figure 3C, RNAs 5-7; Figure 3 – supplement 1E); structures in the 5'-UTR (RNAs 5 and 6) or 3' to the start codon (RNA 7) on their own have 2-3-fold effects on k_{max} relative to the unstructured RNA 4, whereas combining them (RNAs 8 and 9) produces a ≥30-fold effect. These data indicate that structures in both regions synergistically inhibit the rate of mRNA recruitment. This synergy is also reflected in the dramatically reduced recruitment endpoints of RNAs 8-9 seen in the absence of eIF4A (Figure 3A,B, red bars; RNAs 4-7 vs. 8-9). The fact that eIF4A restores recruitment of these RNAs (Figure 3B, RNAs 8-9, black bars), albeit at relatively low recruitment rates, indicates that eIF4A can eventually resolve the synergistic inhibition produced by structures in the 5' and 3' segments of these messages. It is noteworthy, however, that eIF4A gives considerably larger rate enhancements for the mRNAs harboring only native *RPL41A* sequences (RNAs 7 and 10) than those burdened with synthetic hairpins (RNAs 5-6 and 8-9), suggesting that eIF4A is better able to resolve the complex array of relatively less stable structures in *RPL41A* compared to a highly stable local structure in the 5'-UTR.

The 5'-7-methylguanosine cap imposes an eIF4A requirement for structured and unstructured mRNAs

Because eIF4A-dependent ATP hydrolysis is enhanced by eIF4G•4E in our experiments, we next inquired how the 5'-cap influences the requirement for, and activity of, eIF4A in mRNA recruitment. We have previously shown that the 5'-cap enforces the requirement for several eIFs, including eIF4A, in mRNA recruitment (Mitchell et al., 2010). More recent work in the mammalian system provided evidence that the 5'-cap-eIF4E-eIF4G-eIF3-40S network of interactions is required to promote mRNA recruitment via threading of the 5'-end into the 40S entry channel (Kumar et al., 2016). As before, we monitored the kinetics of mRNA recruitment (30 nM PIC conditions) at various concentrations of eIF4A with capped or uncapped versions of mRNAs described above, including RNA 1 (CAA 50-mer), RNA 4 (CAA 250-mer), and RNA 7 (unstructured 5'-UTR with *RPL41A* sequence 3' of the AUG; Figure 4 and Figure 4 – figure supplement 1). As summarized in Figure 4B, the k_{max} observed with saturating eIF4A was comparable with or without the 5'-cap for RNAs 1 and 7, and was 1.5-fold lower with the cap than without it for RNA 4. In contrast, in the absence of eIF4A, the rates of recruitment for uncapped versions of the unstructured model mRNAs 1 and 4 were 3.7- and 2.5-fold higher, respectively, than the rates of the corresponding 5'-capped mRNAs (Figure 4). This effect was even more pronounced for RNA 7, containing natural mRNA sequence 3' of the AUG, which was recruited 15-fold faster when uncapped versus capped in the absence of eIF4A. It is also noteworthy that the rate enhancement provided by eIF4A (Figure 4B, $k_{max}/k_{obs}^{no\ eIF4A}$) is larger in all cases for the capped mRNAs than the uncapped mRNAs, reaching an order of magnitude difference for RNA7, and this effect is due almost entirely to the reduced rate in the absence of eIF4A for the capped versus uncapped mRNAs. Taken together, our data indicate that even for short mRNAs with low structural complexity, the 5'-cap inhibits recruitment in the absence of eIF4A, consistent with our previous observations with a natural mRNA and our proposal that the cap serves, in part, to enforce use of the canonical mRNA recruitment pathway (Mitchell et al., 2010).

DISCUSSION

Fifteen years ago it was suggested that the substrate for eIF4A – *in vivo* – is likely single stranded RNA (Rogers et al., 2002). Since then, high resolution crystal structures, genetics, and biochemical studies provided critical insights into its mechanism of catalysis, alone and in the context of eIF4F (Harms et al., 2014; Hilbert et al., 2011; Lindqvist et al., 2008; Merrick, 2015; Oberer et al., 2005; Schütz et al., 2008). More recently, Next Generation Sequencing (i.e. ribosome profiling) allowed holistic examination of the effects of eIF4A on global translation (Sen et al., 2015) and biochemical techniques gave clues as to how eIF4A and eIF4F may interact with the rest of the recruitment machinery (Gao et al.,

2016; Garcia-Garcia et al., 2015; Kumar et al., 2016). However, the exact role and mechanism of eIF4A in mRNA recruitment to the PIC remain open questions.

Our data demonstrate that ATP hydrolysis by eIF4A stimulates the recruitment of both natural *RPL41A* mRNA, containing only a 24 nt 5'-UTR, and a 50 nt model mRNA that is expected to have little secondary or tertiary structure. We also report that the PIC stimulates the ATPase activity of eIF4A, suggesting that eIF4A, eIF4F, or both interact with the PIC to promote mRNA recruitment, in a manner requiring the i and g subunits of eIF3. We further observed that eIF4A accelerates recruitment of structured as well as unstructured mRNAs, and this acceleration does not correlate with the amount of secondary structure in the 5'-UTR. Instead, the requirement for eIF4A is most pronounced for mRNAs containing structural complexity throughout their sequence. We propose that eIF4A functions to relax the global structures of mRNAs – generated by the ensemble of many, often transient, base pairs and other stabilizing interactions between neighboring and distant parts of the mRNA – to facilitate interaction between the PIC and the 5'-UTR of the message. In addition, the observation that eIF4A accelerates the rate of recruitment of a short, unstructured model mRNA suggests that it may also act to load unwound segments of mRNA into the entry channel of the PIC, either by directly handing them off into the channel or by remodeling the PIC itself. We found that the presence of the cap structure confers a strong requirement for eIF4A for rapid recruitment even for unstructured mRNAs, which is consistent with a recent proposal (Kumar et al., 2016) that cap-eIF4E interaction favors mRNA recruitment via threading of the 5'-end into the 40S entry channel in a manner dependent on eIF4A, eIF4G, and eIF3.

The PIC stimulates eIF4A and eIF4F ATPase activity

In the prevailing model of mRNA recruitment, eIF4F is localized to the 5'-end of the mRNA via the eIF4E-cap interaction, where it collaborates with eIF4B to unwind the mRNA. Consistent with this model, eIF4G and eIF4B were the only proteins known to stimulate eIF4A activity in translation initiation (Hinnebusch, 2014; Mitchell et al., 2011). And yet, given the natural propensity of an mRNA to form structure it is difficult to envision how an mRNA could be unwound by eIF4F and eIF4B, released into the cytoplasm and then bound by the PIC without the mRNA reforming its structure. Moreover, recent work has demonstrated that yeast eIF4B binds the ribosome itself (Walker et al., 2013) and previous evidence suggested that mammalian eIF4B interacts with rRNA (Methot et al., 1996), thus blurring the lines between the PIC and the activated mRNP composed of mRNA, eIF4F and eIF4B. In another proposed model, eIF4F and eIF4B could interact with the PIC, forming a "holo-PIC" (Aitken and Lorsch, 2012) that relaxes the mRNA and attaches to it synchronously. Some support for a model in which eIF4F interacts with the PIC to

promote mRNA recruitment came from hydroxyl radical footprinting experiments that indicate eIF4G binds to the 40S subunit near the eukaryotic expansion segment 6 of the 18S rRNA (Yu et al., 2011). In addition, in mammals (but not *S. cerevisiae*) eIF4G interacts with eIF3, which could serve to bring the eIF4F complex onto the PIC (des Georges et al., 2015). Our observation that the PIC stimulates the ATPase activity of eIF4A, both in the context of the eIF4F complex and in the absence of eIF4G•4E, indicates that eIF4A and eIF4F interact with the PIC, and is consistent with the holo-PIC model.

Our studies of eIF4A ATPase activity demonstrated that nearly all core components of the PIC are necessary for full acceleration of ATP hydrolysis, suggesting that the intact PIC is required for fully productive interaction with eIF4A and eIF4F (Figure 2). The absence of eIFs 2 or 3, or the 40S subunit significantly decreased the rate of ATP hydrolysis, and the presence of the 40S subunit and TC alone gave no stimulation of ATP hydrolysis beyond that afforded by eIF4F. An eIF3 subcomplex comprised of subunits a, b, and c but lacking subunits g and i, resulted in a similar rate decrease as when eIF3 was omitted entirely from the reaction. The g and i subunits of eIF3 have been implicated in mRNA recruitment and scanning (Aitken et al., 2016; Cuchalová et al., 2010; Valásek, 2012), and structural data suggest that they are located near the mRNA entry channel of the 40S subunit, on either the solvent or intersubunit face (Aylett et al., 2015; des Georges et al., 2015; Llacer et al., 2015). The observation that these eIF3 subunits appear at distinct locations near the mRNA entry channel in complexes either containing or lacking mRNA has led to the speculation that they might participate in a large-scale rearrangement of the PIC important for either initial attachment to the mRNA or scanning along it (Llacer et al., 2015; Simonetti et al., 2016). Our observation that the eIF3 g and i subunits are required for full stimulation of eIF4A's ATPase activity is consistent with the possibility that eIF4A is located near the mRNA entry channel, where it can promote mRNA loading onto the PIC (Spirin, 2009).

The mechanism through which the PIC components stimulate eIF4A's ATPase activity is not yet clear. Similar to eIF4G•4E, the PIC (in the absence of eIF4G•4E) increases the V_{max} for ATP hydrolysis by eIF4A. Unlike eIF4G•4E, however, the PIC does not significantly decrease eIF4A's K_m for ATP, suggesting the mechanisms of stimulation are distinct. eIF4G acts as a "soft clamp" that holds the two RecA-like domains of eIF4A in close proximity to each other, in a conformation poised for ATP binding and hydrolysis (Hilbert et al., 2011; Oberer et al., 2005; Schütz et al., 2008). It seems possible that the interaction with one or more components of the PIC also alters the conformation of eIF4A to stimulate its ATPase activity, albeit in a manner distinct from eIF4G•4E that does not enhance binding of ATP. The fact that the PIC stimulates the activity of eIF4A in the absence of eIF4G•4E indicates that the effect does not have to be

mediated through interaction with eIF4G•4E, although it is plausible that the mode of stimulation is different for eIF4A on its own and when it is part of the eIF4F complex.

eIF4A promotes recruitment of all mRNAs regardless of their degree of structure

A number of observations have suggested that the function of eIF4A is to unwind structures in the 5'-UTRs of mRNAs. *In vitro*, eIF4A can unwind model RNA duplexes (Andreou and Klostermeier, 2013b; Blum et al., 1992; Grifo et al., 1983; Lorsch and Herschlag, 1998b; Ray et al., 1985; Rogers et al., 1999, 2001; Seal et al., 1983), albeit at a rate slower than necessary to support the rate of translation initiation *in vivo* (Palmiter, 1975). The factor is required in reconstituted translation systems for 48S PIC formation (Benne and Hershey, 1978; Pestova and Kolupaeva, 2002; Schreier and Staehelin, 1973), and in mammalian extracts the eIF4A-dependence of translation of different reporter mRNAs was correlated with their degree of 5'-UTR structure (Svitkin et al., 2001). On the other hand, eIF4A has also been shown to stimulate initiation *in vitro* on mRNAs with low degrees of 5'-UTR structure (Blum et al., 1992; Pestova and Kolupaeva, 2002), and ribosome profiling studies have shown that the vast majority of mRNAs in yeast display a similar, strong dependence on eIF4A for efficient translation, whereas mRNAs with long, structured 5'-UTRs generally exhibit a special dependence on the helicase Ded1 in addition to their general requirement for eIF4A (Sen et al., 2015). The latter results suggested that eIF4A functions in loading all mRNAs onto the PIC independent of their 5'-UTR structures. Our observation that eIF4A accelerates the recruitment not just of the natural *RPL41A* mRNA and model mRNAs containing secondary structures in their 5'-ends, but also of unstructured mRNAs comprising CAA repeats, supports this proposal.

It is possible that eIF4A, in addition to alleviating structure in mRNA (see below), also plays a role in directing the hand-off of single-stranded mRNA segments to the PIC. It could do this by directly transferring mRNA into the entry channel of the 40S subunit. Another possibility is that eIF4A may directly modulate the conformation of the PIC itself (Figure 5), for example by opening the mRNA entry channel. In fact, a recent report suggests that mammalian eIF4A may be involved in modulating the conformation of the ribosome (Sokabe and Fraser, 2017) and several examples of DEAD-box helicases rearranging ribonucleoprotein complexes exist (Henn et al., 2012; Jankowsky, 2011; Linder and Jankowsky, 2011) including mammalian eIF4AIII, which is critical in formation of Exon Junction Complexes (Andersen et al., 2006; Ballut et al., 2005), and Dhx29, which binds to and is thought to modulate the mammalian ribosome (Hashem et al., 2013; Pisareva et al., 2008). Moreover, the bacterial ribosome has been demonstrated to possess intrinsic helicase activity (Qu et al., 2011; Takyar et al., 2005) and the residues responsible for this activity are

preserved in the eukaryotic ribosome. In fact, we recently demonstrated that the equivalent residues in Rps3 – which is near the 40S latch and interacts with eIF3 – stabilize the PIC:mRNA interaction (Dong et al., 2017). It is thus possible that ATP hydrolysis by eIF4A might contribute to modulating this region, thereby promoting PIC attachment and/or scanning. Both the possibilities that eIF4A directly loads mRNA segments onto the PIC and that it modulates the conformation of the complex are consistent with our observation that the PIC stimulates the ATPase activity of eIF4A.

Global mRNA structure, not just structure in the 5'-UTR, inhibits mRNA recruitment

We observed that addition of native *RPL41A* mRNA sequences 3' of the start codon inhibits recruitment of mRNA to the PIC, even if the 5'-UTR is made up of CAA repeats, and this inhibitory effect is ameliorated by eIF4A (Figure 3, compare RNA 4 to RNA 7). This result is surprising because in the canonical model eIF4A functions to resolve structures in the 5'-UTR. In combination, isolated hairpins in the 5'-UTR and structural complexity 3' of the AUG codon synergistically inhibit mRNA recruitment (Figure 3, RNAs 8 and 9). Together, these results suggest that the global structure of the mRNA is a critical determinant of the efficiency of mRNA recruitment. We envision that the *RPL41A* sequences introduce an ensemble of relatively weak secondary or tertiary interactions that occlude the 5'-UTR and start codon and thus impede PIC attachment and AUG recognition, and that eIF4A can efficiently resolve these structural impediments. In addition, RNAs longer than their persistence length inherently fold back on themselves (Chen et al., 2012) and, by binding to single-stranded segments, eIF4A may serve to increase their persistence length, leading to untangling. It is intriguing that eIF4A was 15- to 20-fold more effective in overcoming the inhibitory effect of the *RPL41A* sequences versus the 5'-UTR hairpins in the RNAs containing one or the other inhibitory element (Figure 3C-D, RNAs 5-7). This could be explained by proposing that eIF4A is more efficient at resolving the relatively weak interactions that contribute to global mRNA structure compared to highly-stable local structures. Indeed, only a handful of native mRNAs are known to possess stable hairpin structures in yeast cells (Rouskin et al., 2014), yet eIF4A is essential for translation of virtually all mRNAs *in vivo*. Moreover, it was shown that Ded1 rather than eIF4A was required to overcome the inhibitory effects of hairpin insertions on reporter mRNA translation *in vivo* (Sen et al., 2015). Combined with these previous findings, our results support a model in which eIF4A acts to disrupt moderately stable, transient interactions throughout an mRNA that sequester the mRNA 5'-UTR or start codon within the global mRNA structure, whereas Ded1 is more effective in resolving stable, local secondary structures in the 5'-UTR or the initiation region of an mRNA.

Our proposal for eIF4A function is consistent with previous work suggesting that other DEAD-box helicases disrupt tertiary RNA interactions rather than unwinding stable hairpins (Pan et al., 2014) and previous reports that eIF4A is a very weak helicase when presented with stable RNA duplexes *in vitro* (Linder and Jankowsky, 2011; Rogers et al., 1999). Ded1 is a much stronger helicase than eIF4A or eIF4F in unwinding the same duplex substrates *in vitro* (Gao et al., 2016). Moreover, it was shown that eIF4A cannot substitute for Ded1, or the mammalian helicase Dhx29, to promote PIC scanning through highly stable hairpins inserted into model unstructured 5'-UTRs in a reconstituted mammalian system. Interestingly, Dhx29 could not substitute for eIF4A in facilitating 48S PIC assembly on native Beta-globin mRNA, supporting the notion of functional diversification of eIF4A versus Ded1 and Dhx29 in different aspects of initiation (Pisareva et al., 2008).

It is intriguing that inserting hairpins into the unstructured 5'-UTRs of our model mRNAs conferred strong inhibitory effects only when *RPL41A* sequences were present 3' of the AUG codon (Figure 3B-C, RNAs 5-6 vs. 8-9), and that the hairpins dramatically increased the inhibition of mRNA recruitment beyond that produced by the *RPL41A* sequences alone. One possible explanation for this strong synergistic effect would be that the hairpins are stabilized by interactions of the unpaired bases in their loops with one or more short stretches of sequences within *RPL41A*. We can also envision that, in the absence of global structure conferred by the *RPL41A* sequences, the PIC can bypass the hairpins in the 5'-UTR and bind directly near the start codon, with the unstructured initiation region slotting into the 40S mRNA binding cleft. This slotting mechanism could be impeded by the presence of *RPL41A* sequences and attendant sequestration of the 5'-UTR within the global mRNA structure, requiring a switch to the scanning mechanism, with the mRNA 5'-end being fed into the entry channel pore (Kumar et al., 2016). The hairpin structures would strongly impede this threading mechanism and the relatively weak helicase activity of eIF4A could only partially overcome this impediment to PIC attachment and AUG recognition.

Perspectives

The work presented here addresses the apparent contradiction between the fact that eIF4A is an essential protein responsible for promoting the translation of virtually all mRNAs *in vivo* (Sen et al., 2015) and its status as one of the weaker RNA helicases known. It is curious that in the presence of related but more robust DEAD-box RNA helicases in the cell, eIF4A is an essential protein and that small changes in its concentration affect the rate of translation (Firczuk et al., 2013). Evolution is clearly capable of achieving more efficient helicase activity, thus the slow catalysis by eIF4A must be either sufficient or advantageous. Our data suggest that eIF4A contributes to mRNA recruitment not

primarily by unwinding stable secondary structures in the 5'-UTR, at which it is relatively inefficient, but by resolving the overall mRNA structure, involving the large ensemble of different conformers stabilized by limited base-pairing and other individual interactions (Figure 5). The result of this structural "untangling" might be to facilitate identification of the 5' end of the mRNA, or the AUG codon, by the PIC. In fact, our observation that the PIC stimulates eIF4A activity suggests that eIF4A or eIF4F might be part of a larger holoPIC complex that couples mRNA relaxation, initial mRNA loading, and possibly even scanning (the latter two processes are not resolved from one another in our assay).

If eIF4A does contribute to translation initiation as a component of the holoPIC, its presence in large excess of all other initiation factors and ribosomal subunits (Firczuk et al., 2013) remains a mystery. Perhaps excess eIF4A plays an additional role by binding to RNA unwound by eIF4F or by more potent helicases such as Ded1 (Firczuk et al., 2013; Gao et al., 2016), or that transiently become single-stranded owing to thermal fluctuations. The slow rate of ATP hydrolysis by eIF4A (k_{cat} of ~0.5 min^{-1}), considerably slower than the estimated rate of initiation *in vivo* (approximately 10 min^{-1})(Palmiter, 1975), might then prove advantageous by increasing the lifetime of eIF4A-mRNA interactions. Considering the >40-fold stimulation of eIF4A ATPase activity by the PIC together with eIF4G•4E observed here, we envision that scanning PICs would promote rapid ATP hydrolysis by such mRNA-bound eIF4A molecules encountered during scanning (Lindqvist et al., 2008), resulting in eIF4A dissociation from the 5'-UTR (Figure 5). This recurring PIC-eIF4A interaction might contribute to scanning processivity by ensuring that single-stranded mRNA is continuously presented at the PIC entry channel; the successive cycles of PIC-eIF4A interaction at the entry channel followed by eIF4A dissociation might also bias the directionality of scanning (Spirin, 2009) (Figure 5). If these mRNA-bound eIF4A•ATP complexes loaded sequentially onto eIF4G prior to ATP hydrolysis, release of mRNA into the entry channel, and dissociation of eIF4A•ADP from eIF4G, the model would be consistent with previous observations that an ATPase deficient mutant of eIF4A acts in a dominant-negative fashion to inhibit translation initiation *in vitro* (Pause et al., 1994), as the mutation would block dissociation of eIF4A molecules from the mRNA when they encounter eIF4G in the scanning PIC, and thereby impede progression through the 5'-UTR. This proposal is a variation on the model originally suggested by Sonenberg, Merrick, and colleagues, in which eIF4A molecules "recycle" through the eIF4F complex in order to promote mRNA recruitment and scanning (Yoder-Hill et al., 1993).

MATERIALS AND METHODS

Materials

ATP, GTP, CTP, and UTP (products 10585, 16800, 14121, 23160, respectively) were purchased from Affymetrix. [α-^{32}P]-GTP was from PerkinElmer (product BLU006H250UC). ATP-γ-S, ADPCP, and ADPNP (products A1388, M7510, and A2647, respectively), S-adenosyl methionine (SAM) (product A7007), and the pyruvate kinase (900-1400 units/mL)/lactate dehydrogenase (600-1000 units/mL) mix from rabbit muscle (product P0294) were from Sigma. NADH disodium salt was from Calbiochem (product 481913). Phosphoenolpyruvate potassium salt was purchased from Chem Impex International, Inc. (product 09711). RiboLock RNase inhibitor was from Thermo Fisher Scientific (product EO0381). The RNeasy RNA purification kit was purchased from Qiagen (product 74106). Exonuclease T was purchased from New England Biolabs (product M0265S). The Abnova Small RNA Marker was purchased from Abnova (product number R0007). SYBR Gold nucleic acid gel stain (product S11494) and Novex 15% TBE-Urea gels (product EC68852BOX) were purchased from Thermo Fisher Scientific. Corning 384-well plates were purchased from VWR (product 3544).

Reagent Preparation

Eukaryotic initiation factors – eIFs 1, 1A, 2, 3, 4A, 4B, 4E•4G, and 5 – as well as mRNA were prepared as described previously (Walker et al., 2013); see Supplementary Methods for more detail. $tRNA_i$ was charged with methionine as described previously (Walker and Fredrick, 2008). Following charging, Met-$tRNA_i$ was separated from contaminating ATP and other nucleotides (left over from the charging reaction) on a 5 mL General Electric (GE) desalting column equilibrated in 30 mM Sodium Acetate (NaOAc), pH 5.5. This step was essential in order to measure the ATP dependence of mRNA recruitment and to accurately control the concentration of ATP in experiments. The Met-$tRNA_i$ and free nucleotide peaks were confirmed with individual standards prepared identically to a charging reaction. Eluted Met-$tRNA_i$ was precipitated with 3 volumes of 100% ethanol at –20°C overnight, pelleted, and resuspended in 30 mM NaOAc, pH 5.5.

mRNA capping

mRNAs were capped as described previously (Aitken et al., 2016). Briefly, RNAs 2-10 at 5 μM were combined with 50 μM GTP, 0.67 μM [α-^{32}P]-GTP, 100 μM S-adenosyl methionine (SAM), 1 U/μl RiboLock, and 0.15 μM D1/D12 vaccinia virus capping enzyme. RNA 1 was present at 50 μM in the reaction in the presence of 100 μM GTP,

with all other conditions identical. Reactions were incubated at 37 °C for 90 minutes and purified using the RNeasy (Qiagen) RNA purification kit.

mRNA Recruitment Assay

In vitro mRNA recruitment assays were carried out as described previously with minor modifications (Aitken et al., 2016; Walker et al., 2013). All reactions were carried out at 26°C in "Recon" buffer containing 30 mM HEPES•KOH, pH 7.4, 100 mM KOAc, 3 mM $Mg(OAc)_2$, and 2 mM DTT. 15 µl reactions contained final concentrations of 500 nM GDPNP•Mg^{2+}, 300 nM eIF2, 300 nM Met-$tRNA_i$, 1 µM eIF1, 1 µM eIF1A, 30 nM 40S ribosomal subunits, 300 nM eIF3, 5 µM eIF4A, 50 nM eIF4G•eIF4E, 300 nM eIF4B, and 1 U/µL Ribolock RNase inhibitor (Thermo). To form the ternary complex (TC), GDPNP and eIF2 were incubated for 10 minutes, Met-$tRNA_i$ was then added to the reaction and incubated an additional 7 minutes. The remainder of the components, except mRNA and ATP, were added to the TC and incubated for an additional 10 minutes to allow complex formation. Reactions were initiated with a mix containing final concentrations of 15 nM mRNA and ATP•Mg^{2+}. Experiments varying the concentration of eIF4A were carried out in the presence of 5 mM ATP. Experiments varying ATP were carried out in the presence of 5 µM eIF4A. To take timepoints, 2 µl reaction aliquots were combined with 1 µl of 0.02% bromophenol blue and xylene cyanol dye in 40% sucrose containing a final concentration of a 25-fold excess of unlabeled mRNA (cold chase), identical to the labeled mRNA for that reaction. Two µl of the chased reaction were immediately loaded and resolved on a native 4% (37.5:1) polyacrylamide gel using a Hoefer SE260 Mighty Small II Deluxe Mini Vertical Electrophoresis Unit at a potential of 200 volts for 50 minutes. The electrophoresis unit was cooled to 22°C by a circulating water bath. Gels and running buffer contained 34 mM Tris Base, 57 mM HEPES, 1 mM EDTA, and 25 mM $MgCl_2$ ("THEM"). Gels were exposed to a phosphor plate overnight at –20°C, the plates visualized on a GE Typhoon 9500 FLA, and the fraction of recruited mRNA bands (48S complex) versus the total signal in the lane was quantified using ImageQuant software. Data were plotted and fit using KaleidaGraph 4.5 software. Recruitment time courses were fit to a single exponential rate equation: $y = A*(1-\exp(-k_{obs}*t))$, where t is time, A is amplitude, and k_{obs} is the observed rate constant. Observed rates were plotted against the concentration of the titrant and fit to a hyperbolic equation: $y = b+((k_{max}*x)/(K_{1/2}+x))$ where x is the concentration of the titrant, k_{max} is the maximal observed rate of mRNA recruitment when the reaction is saturated by the factor titrated (e.g. eIF4A), $K_{1/2}$ is the concentration of the factor required to achieve $\frac{1}{2}V_{max}$, and b is the rate in the absence of the titrated factor (i.e., the y-intercept).

NADH-coupled ATPase Assay

The NADH-coupled ATPase assay was adapted from previously described methods with some modifications (Bradley and De La Cruz, 2012; Kiianitsa et al., 2003). All ATPase experiments were carried out in 384-well Corning 3544 plates on a Tecan Infinite M1000PRO microplate reader at 26°C. Using a standard curve we determined that a 10 μL reaction with 1 mM NADH on a Corning 3544 microplate gives an absorbance of 1.23 Optical Density of 340 nm light (OD_{340}) in the microplate reader. OD_{340} was measured every 20 seconds for 40 minutes, plotted vs. time for individual reactions, and fit to y = mx + b where m is the slope, x is time in minutes, and b is the y-intercept. Thus, m is OD_{340} of NADH/min. It follows that,

$$\frac{|m|\ \text{OD of NADH/min}}{1.23\ \text{OD of NADH/1mM NADH}} = \text{mM NADH/min}$$

Note that the absolute value of m (|m|) was used because the slope is a negative value due to loss of absorbance over time. NADH consumed is stoichiometric with ATP regenerated thus, mM NADH/min = mM ATP/min.

"30 nM PIC:" 12 μl reactions (final volume) were at the same final concentrations as described above in the mRNA Recruitment Assay section: 500 nM GDPNP•Mg^{2+}, 300 nM eIF2, 300 nM Met-$tRNA_i$, 1 μM eIF1, 1 μM eIF1A, 30 nM 40S ribosomal subunits, 300 nM eIF3, 5 μM eIF4A, 50 nM eIF4G•eIF4E, 300 nM eIF4B, and 1 U/μL Ribolock RNase Inhibitor. PICs were formed at 2x of the final concentration in 1x Recon buffer, in the absence of mRNA and ATP. Subsequently, the PICs were combined with the Reporter Mix (added as a 10x stock of the final concentrations all in 1x Recon buffer) resulting in concentrations in the final reaction of 2.5 mM phosphoenolpyruvate, 1 mM NADH, and a 1/250 dilution of the pyruvate kinase (600-1,000 units/mL) and lactate dehydrogenase (900-1400 units/mL) mix (PK/LDH mix). Reactions were brought up to volume with 1x Recon buffer, such that when they were initiated by addition of mRNA (added as a 10x stock of the final concentration in 1 x Recon) and ATP•Mg^{2+} (added as a 4x stock of the final concentration in 1x Recon buffer) the total reaction volume was 12 μl. 10 μl of the reaction were then immediately transferred to the microplate for analysis by the Tecan plate reader and changes in absorbance of 340 nm light were monitored over time, taking readings every 20 seconds for 40 minutes. Because the assay measures the reaction velocity (i.e. slope of a straight line), the lag in time between initiating the reaction and start of the measurements by the plate reader has no effect on the results. Initiating the reactions using an injection, capable of monitoring rapid kinetics did not reveal any different results; i.e., there was no evidence of a "burst" phase in the initial part of the reaction. Increasing or decreasing the concentration of the PK/LDH mix by 3-fold did not influence the

observed rate of ATP hydrolysis (Figure 2 – figure supplement 1A), indicating that the rate of NADH oxidation is not limited by PK/LDH activity. Also, when ATP, eIF4A, or PK/LDH was absent from the reaction, there was no change in absorbance at 340 nm over 1 hour.

"0.5 μM PIC:" Reactions were carried out identically as described in the "30 nM PIC" above except the concentrations in the final reaction were as follows: 1 mM GDPNP•Mg^{2+}, 500 nM eIF2, 500 nM Met-$tRNA_i$, 1 μM eIF1, 1 μM eIF1A, 500 nM 40S ribosomal subunits, 500 nM eIF3, 5 μM eIF4A, 500 nM eIF4G•4E, 500 nM eIF4B, 500 nM eIF5, 5 mM ATP•Mg^{2+}, 500 nM mRNA, and 1 U/μl RiboLock RNase inhibitor.

Exonuclease T RNA Digest

In a 20 μl reaction 0.5 pmol/μl of RNA was incubated with 0.75 U/μl of RNase Exonuclease T in 1x NEB buffer 4 at 26°C for 18 hours. RNA (4 pmol total RNA per lane) was loaded and resolved on a Novex 15% Tris Borate EDTA Urea gel and stained with SYBR Gold nucleic acid gel stain, diluted 1/10,000, for 5 minutes and visualized on a General Electric Typhoon FLA 9500.

ACKNOWLEDGMENTS

The authors would like to acknowledge Tom Dever and Nicholas Guydosh for their thoughtful and critical suggestions. This work was supported by the Intramural Research Program (JRL and AGH) of the National Institutes of Health (NIH).

COMPETING INTERESTS

The authors declare no competing interests.

REFERENCES

Acker, M.G., Kolitz, S.E., Mitchell, S.F., Nanda, J.S., and Lorsch, J.R. (2007). Reconstitution of yeast translation initiation. Methods Enzymol. *430*, 111–145.

Acker, M.G., Shin, B.-S., Nanda, J.S., Saini, A.K., Dever, T.E., and Lorsch, J.R. (2009). Kinetic analysis of late steps of eukaryotic translation initiation. J. Mol. Biol. *385*, 491–506.

Aitken, C.E., and Lorsch, J.R. (2012). A mechanistic overview of translation initiation in eukaryotes. Nat. Struct. Mol. Biol. *19*, 568–576.

Aitken, C.E., Beznosková, P., Vlčkova, V., Chiu, W.-L., Zhou, F., Valášek, L.S., Hinnebusch, A.G., and Lorsch, J.R. (2016). Eukaryotic translation initiation factor 3 plays distinct roles at the mRNA entry and exit channels of the

ribosomal preinitiation complex. Elife *5*, 1–37.
Algire, M. a, Maag, D., and Lorsch, J.R. (2005). Pi release from eIF2, not GTP hydrolysis, is the step controlled by start-site selection during eukaryotic translation initiation. Mol. Cell *20*, 251–262.
Altman, M., Blum, S., Wilson, T., and Trachsel, H. (1990). The 5'-leader sequence of tobacco mosaic virus RNA mediates initiation-factor-4E-independent, but still initiation-factor-4A-dependent translation in yeast extracts. Gene *91*, 127–129.
Andersen, C.B.F., Ballut, L., Johansen, J.S., Chamieh, H., Nielsen, K.H., Oliveira, C.L.P., Pedersen, J.S., Séraphin, B., Hir, H. Le, and Andersen, G.R. (2006). Structure of the Exon Junction Core Complex with a Trapped DEAD-Box ATPase Bound to RNA. Science *313*, 1968–1972.
Andreou, A.Z., and Klostermeier, D. (2013a). The DEAD-box helicase eIF4A: paradigm or the odd one out? RNA Biol. *10*, 19–32.
Andreou, A.Z., and Klostermeier, D. (2013b). SUPP eIF4B and eIF4G Jointly Stimulate eIF4A ATPase and Unwinding Activities by Modulation of the eIF4A Conformational Cycle. J. Mol. Biol.
Andreou, A.Z., and Klostermeier, D. (2014). eIF4B and eIF4G Jointly Stimulate eIF4A ATPase and Unwinding Activities by Modulation of the eIF4A Conformational Cycle. J. Mol. Biol. *426*, 51–61.
Aylett, C.H.S., Boehringer, D., Erzberger, J.P., Schaefer, T., and Ban, N. (2015). Structure of a Yeast 40S–eIF1–eIF1A–eIF3–eIF3j initiation complex. Nat Struct Mol Biol *22*, 269–271.
Ballut, L., Marchadier, B., Baguet, A., Tomasetto, C., Séraphin, B., and Le Hir, H. (2005). The exon junction core complex is locked onto RNA by inhibition of eIF4AIII ATPase activity. Nat. Struct. Mol. Biol. *12*, 861–869.
Benne, R., and Hershey, J.W. (1978). The mechanism of action of protein synthesis initiation factors from rabbit reticulocytes. J. Biol. Chem. *253*, 3078–3087.
Blum, S., Schmid, S.R., Pause, A., Buser, P., Linder, P., Sonenberg, N., and Trachsel, H. (1992). ATP hydrolysis by initiation factor 4A is required for translation initiation in Saccharomyces cerevisiae. Proc. Natl. Acad. Sci. U. S. A. *89*, 7664–7668.
Bradley, M.J., and De La Cruz, E.M. (2012). Analyzing ATP utilization by DEAD-Box RNA helicases using kinetic and equilibrium methods. Methods Enzymol. *511*, 29–63.
Chen, H., Meisburger, S.P., Pabit, S. a., Sutton, J.L., Webb, W.W., and Pollack, L. (2012). Ionic strength-dependent persistence lengths of single-stranded RNA and DNA. Proc. Natl. Acad. Sci. *109*, 799–804.
Cuchalová, L., Kouba, T., Herrmannová, A., Dányi, I., Chiu, W.-L., and Valásek, L. (2010). The RNA recognition motif of eukaryotic translation initiation factor 3g (eIF3g) is required for resumption of scanning of posttermination ribosomes for reinitiation on GCN4 and together with eIF3i stimulates linear scanning. Mol. Cell. Biol. *30*, 4671–4686.
Das, S., Maiti, T., Das, K., and Maitra, U. (1997). Specific Interaction of Eukaryotic Translation Initiation Factor 5 (eIF5) with the Beta-Subunit of eIF2. J. Biol. Chem. *272*, 31712–31718.
Das, S., Ghosh, R., and Maitra, U. (2001). Eukaryotic Translation Initiation Factor 5 Functions as a GTPase-activating Protein. J. Biol. Chem. *276*, 6720–6726.
Deutscher, M.P., Marlor, C.W., and Zaniewski, R. (1984). Ribonuclease T: new exoribonuclease possibly involved in end-turnover of tRNA. Proc. Natl. Acad. Sci. U. S. A. *81*, 4290–4293.
Dever, T.E., Kinzy, T.G., and Pavitt, G.D. (2016). Mechanism and regulation of protein synthesis in Saccharomyces cerevisiae. Genetics *203*, 65–107.
Dong, J., Aitken, C.E., Thakur, A., Shin, B.-S., Lorsch, J.R., and Hinnebusch, A.G. (2017). Rps3/uS3 promotes mRNA binding at the 40S ribosome entry channel and stabilizes preinitiation complexes at start codons. Proc. Natl. Acad. Sci. *114*, E2126–E2135.
Fekete, C.A., Mitchell, S.F., Cherkasova, V.A., Applefield, D., Algire, M.A., Maag, D., Saini, A.K., Lorsch, J.R., and Hinnebusch, A.G. (2007). N- and C-terminal residues of eIF1A have opposing effects on the fidelity of start codon selection. EMBO J. *26*, 1602–1614.
Fersht, A. (1999). Structure and Mechanism in Protein Science (New York, NY: W. H. Freeman and Company).
Firczuk, H., Kannambath, S., Pahle, J., Claydon, A., Beynon, R., Duncan, J., Westerhoff, H., Mendes, P., and McCarthy, J.E. (2013). An in vivo control map for the eukaryotic mRNA translation machinery.
Gao, Z., Putnam, A.A., Bowers, H.A., Guenther, U.-P., Ye, X., Kindsfather, A., Hilliker, A.K., and Jankowsky, E. (2016). Coupling between the DEAD-box RNA helicases Ded1p and eIF4A. Elife *5*, 1–22.

Garcia-Garcia, C., Frieda, K.L., Feoktistova, K., Fraser, C.S., and Block, S.M. (2015). Factor-dependent processivity in human eIF4A DEAD-box helicase. Science *348*, 1486–1488.

des Georges, A., Dhote, V., Kuhn, L., Hellen, C.U.T., Pestova, T. V, Frank, J., and Hashem, Y. (2015). Structure of mammalian eIF3 in the context of the 43S preinitiation complex. Nature *525*, 491–495.

Grifo, J.A., Tahara, S.M., Morgan, M.A., Shatkin, A.J., and Merrick, W.C. (1983). New initiation factor activity required for globin mRNA translation. J. Biol. Chem. *258*, 5804–5810.

von der Haar, T., and McCarthy, J.E.G. (2002). Intracellular translation initiation factor levels in Saccharomyces cerevisiae and their role in cap-complex function. Mol. Microbiol. *46*, 531–544.

Halder, S., and Bhattacharyya, D. (2013). RNA structure and dynamics: A base pairing perspective. Prog. Biophys. Mol. Biol. *113*, 264–283.

Harms, U., Andreou, A.Z., Gubaev, A., and Klostermeier, D. (2014). eIF4B, eIF4G and RNA regulate eIF4A activity in translation initiation by modulating the eIF4A conformational cycle. Nucleic Acids Res. *42*, 7911–7922.

Hashem, Y., des Georges, A., Dhote, V., Langlois, R., Liao, H.Y., Grassucci, R.A., Hellen, C.U.T., Pestova, T. V, and Frank, J. (2013). Structure of the mammalian ribosomal 43S preinitiation complex bound to the scanning factor DHX29. Cell *153*, 1108–1119.

Henn, A., Bradley, M.J., and De La Cruz, E.M. (2012). ATP utilization and RNA conformational rearrangement by DEAD-box proteins. Annu. Rev. Biophys. *41*, 247–267.

Hilbert, M., Kebbel, F., Gubaev, A., and Klostermeier, D. (2011). eIF4G stimulates the activity of the DEAD box protein eIF4A by a conformational guidance mechanism. Nucleic Acids Res. *39*, 2260–2270.

Hinnebusch, A.G. (2014). The Scanning Mechanism of Eukaryotic Translation Initiation. Annu. Rev. Biochem. *83*, 779–812.

Hussain, T., Llácer, J.L., Fernández, I.S., Munoz, A., Martin-Marcos, P., Savva, C.G., Lorsch, J.R., Hinnebusch, A.G., and Ramakrishnan, V. (2014). Structural Changes Enable Start Codon Recognition by the Eukaryotic Translation Initiation Complex. Cell *159*, 597–607.

Jankowsky, E. (2011). RNA helicases at work: binding and rearranging. Trends Biochem. Sci. *36*, 19–29.

Jivotovskaya, A., Valášek, L., Hinnebusch, A.G., and Nielsen, K.H. (2006). Eukaryotic Translation Initiation Factor 3 (eIF3) and eIF2 Can Promote mRNA Binding to 40S Subunits Independently of eIF4G in Yeast. Mol. Cell. Biol. *26*, 1355–1372.

Kiianitsa, K., Solinger, J.A., and Heyer, W.-D. (2003). NADH-coupled microplate photometric assay for kinetic studies of ATP-hydrolyzing enzymes with low and high specific activities. Anal. Biochem. *321*, 266–271.

Kumar, P., Hellen, C.U.T., and Pestova, T. V (2016). Toward the mechanism of eIF4F-mediated ribosomal attachment to mammalian capped mRNAs. Genes Dev *30*, 1573–1588.

Linder, P., and Jankowsky, E. (2011). From unwinding to clamping - the DEAD box RNA helicase family. Nat. Rev. Mol. Cell Biol. *12*, 505–516.

Linder, P., Lasko, P.F., Ashburner, M., Leroy, P., Nielsen, P.J., Nishi, K., Schnier, J., and Slonimski, P.P. (1989). Birth of the D-E-A-D box. Nature *337*, 121–122.

Lindqvist, L., Imataka, H., and Pelletier, J. (2008). Cap-dependent eukaryotic initiation factor-mRNA interactions probed by cross-linking. RNA *14*, 960–969.

Liu, F., Putnam, A., and Jankowsky, E. (2008). ATP hydrolysis is required for DEAD-box protein recycling but not for duplex unwinding. Proc. Natl. Acad. Sci. *51*, 20209–20214.

Llacer, J.L., Hussain, T., Marler, L., Aitken, C.E., Thakur, A., Lorsch, J.R., Hinnebusch, A.G., and Ramakrishnan, V. (2015). Conformational Differences between Open and Closed States of the Eukaryotic Translation Initiation Complex. Mol. Cell *59*, 399–412.

Lorsch, J., and Herschlag, D. (1998a). The DEAD box protein eIF4A. 2. A cycle of nucleotide and RNA-dependent conformational changes. Biochemistry *2960*, 2194–2206.

Lorsch, J.R., and Herschlag, D. (1998b). The DEAD box protein eIF4A. 1. A minimal kinetic and thermodynamic framework reveals coupled binding of RNA and nucleotide. Biochemistry *37*, 2180–2193.

Maag, D., Fekete, C. a, Gryczynski, Z., and Lorsch, J.R. (2005). A conformational change in the eukaryotic translation preinitiation complex and release of eIF1 signal recognition of the start codon. Mol. Cell *17*, 265–275.

Maag, D., Algire, M.A., and Lorsch, J.R. (2006). Communication between eukaryotic translation initiation factors 5 and

1A within the ribosomal pre-initiation complex plays a role in start site selection. J. Mol. Biol. *356*, 724–737.
Merrick, W.C. (2015). eIF4F: A Retrospective. J. Biol. Chem. *290*, 24091–24099.
Methot, N., Pickett, G., Keene, J.D., and Sonenberg, N. (1996). In vitro RNA selection identifies RNA ligands that specifically bind to eukaryotic translation initiation factor 4B: the role of the RNA remotif. RNA *2*, 38–50.
Mitchell, S.F., Walker, S.E., Algire, M.A., Park, E., Hinnebusch, A.G., and Lorsch, J.R. (2010). The 5′-7-Methylguanosine Cap on Eukaryotic mRNAs Serves Both to Stimulate Canonical Translation Initiation and to Block an Alternative Pathway. Mol. Cell *39*, 950–962.
Mitchell, S.F., Walker, S.E., Rajagopal, V., Aitken, C.E., and Lorsch, J.R. (2011). Recruiting knotty partners: The roles of translation initiation factors in mRNA recruitment to the eukaryotic ribosome. In Ribosomes. Springer Vienna, pp. 155–169.
Oberer, M., Marintchev, A., and Wagner, G. (2005). Structural basis for the enhancement of eIF4A helicase activity by eIF4G. Genes Dev. *19*, 2212–2223.
Özeş, A.R., Feoktistova, K., Avanzino, B.C., and Fraser, C.S. (2011). Duplex unwinding and ATPase activities of the DEAD-box helicase eIF4A are coupled by eIF4G and eIF4B. J. Mol. Biol. *412*, 674–687.
Palmiter, R.D. (1975). Quantitation of parameters that determine the rate of ovalbumin synthesis. Cell *4*, 189–197.
Pan, C., Potratz, J.P., Cannon, B., Simpson, Z.B., Ziehr, J.L., Tijerina, P., and Russell, R. (2014). DEAD-Box Helicase Proteins Disrupt RNA Tertiary Structure Through Helix Capture. PLoS Biol. *12*, 1–10.
Park, E.-H., Walker, S.E., Zhou, F., Lee, J.M., Rajagopal, V., Lorsch, J.R., and Hinnebusch, A.G. (2013). Yeast eukaryotic initiation factor 4B (eIF4B) enhances complex assembly between eIF4A and eIF4G in vivo. J. Biol. Chem. *288*, 2340–2354.
Parsyan, A., Svitkin, Y., Shahbazian, D., Gkogkas, C., Lasko, P., Merrick, W.C., and Sonenberg, N. (2011). mRNA helicases: the tacticians of translational control. Nat. Rev. Mol. Cell Biol. *12*, 235–245.
Passmore, L.A., Schmeing, T.M., Maag, D., Applefield, D.J., Acker, M.G., Algire, M. a, Lorsch, J.R., and Ramakrishnan, V. (2007). The eukaryotic translation initiation factors eIF1 and eIF1A induce an open conformation of the 40S ribosome. Mol. Cell *26*, 41–50.
Paulin, F.E., Campbell, L.E., O'Brien, K., Loughlin, J., and Proud, C.G. (2001). Eukaryotic translation initiation factor 5 (eIF5) acts as a classical GTPase-activator protein. Curr. Biol. *11*, 55–59.
Pause, A., Methot, N., and Svitkin, Y. (1994). Dominant negative mutants of mammalian translation initiation factor elF-4A define a critical role for elF-4F in cap-dependent and cap-independent initiation of translation. EMBO J. *1*.
Peck, M., and Herschlag, D. (2003). Adenosine 5′-O-(3-thio)triphosphate (ATPγS) is a substrate for the nucleotide hydrolysis and RNA unwinding activities of eukaryotic translation initiatino factor 4A. RNA.
Pelletier, J., and Sonenberg, N. (1985). Insertion mutagenesis to increase secondary structure within the 5' noncoding region of a eukaryotic mRNA reduces translational efficiency. Cell *40*, 515–526.
Pestova, T. V, and Kolupaeva, V.G. (2002). The roles of individual eukaryotic translation initiation factors in ribosomal scanning and initiation codon selection. Genes Dev. *16*, 2906–2922.
Pestova, T. V, Borukhov, S.I., and Hellen, C.U. (1998). Eukaryotic ribosomes require initiation factors 1 and 1A to locate initiation codons. Nature *394*, 854–859.
Pisareva, V.P., Pisarev, A. V, Komar, A.A., Hellen, C.U.T., and Pestova, T. V (2008). Translation initiation on mammalian mRNAs with structured 5'UTRs requires DExH-box protein DHX29. Cell *135*, 1237–1250.
Qu, X., Wen, J.-D., Lancaster, L., Noller, H.F., Bustamante, C., and Tinoco, I. (2011). The ribosome uses two active mechanisms to unwind messenger RNA during translation. Nature *475*, 118–121.
Rajagopal, V., Park, E.-H., Hinnebusch, A.G., and Lorsch, J.R. (2012). Specific Domains in Yeast Translation Initiation Factor eIF4G Strongly Bias RNA Unwinding Activity of the eIF4F Complex toward Duplexes with 5'-Overhangs. J. Biol. Chem. *287*, 20301–20312.
Ray, B.K., Lawson, T.G., Kramer, J.C., Cladaras, M.H., Grifo, J.A., Abramson, R.D., Merrick, W.C., and Thach, R.E. (1985). ATP-dependent unwinding of messenger RNA structure by eukaryotic initiation factors. J. Biol. Chem. *260*, 7651–7658.
Rogers, G., Richter, N., and Merrick, W. (1999). Biochemical and Kinetic Characterization of the RNA Helicase Activity of Eukaryotic Initiation Factor 4A. J. Biol. Chem. *274*, 12236–12244.
Rogers, G.W., Lima, W.F., and Merrick, W.C. (2001). Further characterization of the helicase activity of eIF4A.

Substrate specificity. J. Biol. Chem. *276*, 12598–12608.
Rogers, G.W.J., Komar, A.A., and Merrick, W.C. (2002). eIF4A: The Godfather of the DEAD Box Helicases. Prog. Nucleic Acid Res. Mol. Biol. *72*, 307–331.
Rouskin, S., Zubradt, M., Washietl, S., Kellis, M., and Weissman, J.S. (2014). Genome-wide probing of RNA structure reveals active unfolding of mRNA structures in vivo. Nature *505*, 701–705.
Schreier, M.H., and Staehelin, T. (1973). Translation of Rabbit Hemoglobin Messenger RNA In Vitro with Purified and Partially Purified Components from Brain or Liver of Different Species. Proc. Natl. Acad. Sci. U. S. A. *70*, 462–465.
Schreier, M., Erni, B., and Staehelin, T. (1977). Purification and Characterization of Seven Initiation Factors. J. Mol. Biol. *116*, 727–753.
Schütz, P., Bumann, M., Oberholzer, A.E., Bieniossek, C., Trachsel, H., Altmann, M., and Baumann, U. (2008). Crystal structure of the yeast eIF4A-eIF4G complex: an RNA-helicase controlled by protein-protein interactions. Proc. Natl. Acad. Sci. *105*, 9564–9569.
Seal, S.N., Schmidt, A., and Marcus, A. (1983). Eukaryotic initiation factor 4A is the component that interacts with ATP in protein chain initiation. Proc Natl Acad Sci U S A *80*, 6562–6565.
Sen, N.D., Zhou, F., Ingolia, N.T., and Hinnebusch, A.G. (2015). Genome-wide analysis of translational efficiency reveals distinct but overlapping functions of yeast DEAD-box RNA helicases Ded1 and eIF4A. Genome Res. *25*, 1196–1205.
Sen, N.D., Zhou, F., Harris, M.S., Ingolia, N.T., and Hinnebusch, A.G. (2016). eIF4B stimulates translation of long mRNAs with structured 5′ UTRs and low closed-loop potential but weak dependence on eIF4G. Proc. Natl. Acad. Sci. 201612398.
Simonetti, A., Querido, J.B., Myasnikov, A.G., Mancera-Martinez, E., Renaud, A., Kuhn, L., and Hashem, Y. (2016). eIF3 Peripheral Subunits Rearrangement after mRNA Binding and Start-Codon Recognition. Mol. Cell *63*, 206–217.
Sobczak, K., Michlewski, G., De Mezer, M., Kierzek, E., Krol, J., Olejniczak, M., Kierzek, R., and Krzyzosiak, W.J. (2010). Structural diversity of triplet repeat RNAs. J. Biol. Chem. *285*, 12755–12764.
Sokabe, M., and Fraser, C.S. (2017). A helicase-independent activity of eIF4A in promoting mRNA recruitment to the human ribosome. Proc. Natl. Acad. Sci.
Spirin, A.S. (2009). How does a scanning ribosomal particle move along the 5'-untranslated region of eukaryotic mRNA? Brownian Ratchet model. Biochemistry *48*, 10688–10692.
Svitkin, Y.Y. V, Pause, A., Haghighat, A., Pyronnet, S., Witherell, G., Belsham, G.J., and Sonenberg, N. (2001). The requirement for eukaryotic initiation factor 4A (eIF4A) in translation is in direct proportion to the degree of mRNA 5' secondary structure. RNA *7*, 382–394.
Takyar, S., Hickerson, R.P., and Noller, H.F. (2005). mRNA helicase activity of the ribosome. Cell *120*, 49–58.
Valásek, L.S. (2012). "Ribozoomin" – translation initiation from the perspective of the ribosome-bound eukaryotic initiation factors (eIFs). Curr. Protein Pept. Sci. *13*, 305–330.
Walker, S.E., and Fredrick, K. (2008). Preparation and evaluation of acylated tRNAs. Methods *44*, 81–86.
Walker, S.E., Zhou, F., Mitchell, S.F., Larson, V.S., Valasek, L., Hinnebusch, A.G., and Lorsch, J.R. (2013). Yeast eIF4B binds to the head of the 40S ribosomal subunit and promotes mRNA recruitment through its N-terminal and internal repeat domains. RNA *19*, 191–207.
Yoder-Hill, J., Pause, A., Sonenberg, N., and Merrick, W.C. (1993). The p46 subunit of eukaryotic initiation factor (eIF)-4F exchanges with eIF-4A. J. Biol. Chem. *268*, 5566–5573.
Yu, Y., Abaeva, I.S., Marintchev, A., Pestova, T. V., and Hellen, C.U.T. (2011). Common conformational changes induced in type 2 picornavirus IRESs by cognate trans-acting factors. Nucleic Acids Res. *39*, 4851–4865.
Zeng, Y., and Cullen, B.R. (2004). Structural requirements for pre-microRNA binding and nuclear export by Exportin 5. Nucleic Acids Res. *32*, 4776–4785.
Zuker, M. (2003). Mfold web server for nucleic acid folding and hybridization prediction. Nucleic Acids Res. *31*, 3406–3415.

SUPPLEMENTARY METHODS

RNAs used in the study:

RNA 1 was transcribed using the T7 RNA Polymerase and a DNA template while RNAs 2-10 were transcribed from a plasmid digested with a restriction nuclease at the 3'-end of the desired DNA template (i.e. run-off transcription) exactly as described previously (Acker et al., 2007).

RNA	DNA Template name	DNA Template Sequence (5'-3') complementary "clamp" DNA oligomer annealed to the region in bold	Resulting T7 transcribed RNA sequence (5'-3') purified by denaturing acrylamide gel electrophoresis
1	midAUG 23	TCGACTTTGTTGTTGTTGTTGTTCCATT TGTTGTTGTTGTTGTTGTTG**CCTATAG TGAGTCGTATTACATATGCGTGTTACC**	GGCAACAACAACAACAACAACAA**AUG**GAACAACAACAAC AACAAAGUCGA

RNA	Plasmid name	Cloning Vector	Digested for T7 Polymerase run-off transcription	Resulting RNA sequence (5'-3') made by T7 RNA Polymerase run-off transcription and purified by denaturing acrylamide gel electrophoresis
2	SL25-0	pBluescript II KS (+)	SalI-HF	GGAAAGAAUUCACUUAAGCAACAAA**AUG**GAAACAAACAAACAAACAAACAAAC AAAACUAGUCAACAACAACAACAACAACAACAACAACAACAACAACAACAACAA CAACAACAACAACAACAACAACAACAACAACAACAACAACAACAACAACAACAACAA CAACAACAACAACAACAACAACAACAACAACAACAACAACAACAACAACAACAACAA CAACAACAACAACAACAACAACAAACAAACAAAG
3	SL150-0	pBluescript II KS (+)	SalI-HF	GGAAAGAAUUCACAACAACAACAACAACAACAACAACAACAACAACAACAACAACA ACAACAACAACAACAACUUAAGCAACAACAACAACAACAACAACAACAACAACAACA AUUGAAACAACAACAACAACAACAACAACAACAACAACAACAAAAA**AUG**GAAACAA ACAAACAAACAAACAAACAAAACUAGUCAACAACAACAACAACAACAACAACAACAA CAACAACAACAACAACAACAACAACAACAACAACAAAG
4	CAA617	pUC57	SspI-HF	GGAACAACAACAACAACAACAACAACAACAACAACAACAACAACAACAACAACAACA ACAACAACAAAAA**AUG**AGAGAACAACAACAACAACAACAACAACAACAACAAC AACAACAACAACAACAACAACAACAACAACAACAACAACAACAACAACAACAACAAC AACAACAACAACAACAACAACAACAACAACAACAACAACAACAACAACAACAACAAC AACAACAACAACAACAACAACAACAACAACAACAAAAU

RNA	Plasmid name	Cloning Vector	Digested for T7 Polymerase run-off transcription	Resulting RNA sequence (5'-3') made by T7 RNA Polymerase run-off transcription and purified by denaturing acrylamide gel electrophoresis
5	CAA663	pUC57	SspI-HF	GGAAAGAAUUGCCAUCUUGGCAAUUCAACAACAACAACAACAACAACAACAACAAC AACAACAACAACAACAACAACAACAACAAAAA**AUG**AGAGAACAACAACAACAACAA CAACAACAACAACAACAACAACAACAACAACAACAACAACAACAACAACAACAACAA CAACAACAACAACAACAACAACAACAACAACAACAACAACAACAACAACAACAACAA CAACAACAACAACAACAACAACAACAACAACAACAACAACAACAACAACAACAACAA AAU
6	CAA659	pUC57	SspI-HF	GGAAACAACAACAACAACAACAACAACAACAACAACAACAACAACAACAAGAAUUGCCA UCUUGGCAAUUCCAACAACAACAACAAAAAA**AUG**AGAGAACAACAACAACAACA ACAACAACAACAACAACAACAACAACAACAACAACAACAACAACAACAACAACAACA ACAACAACAACAACAACAACAACAACAACAACAACAACAACAACAACAACAACAACA ACAACAACAACAACAACAACAACAACAACAACAACAACAACAACAACAACAACAACA AAU
7	FJZ617	pBluescript II KS (+)	SalI-HF	GGAAAGAAUUCAACAACAACAACAACAACAACAACAACAACAACAACAACAACAAC AACAACAACAAAAA**AUG**AGAGCCAAGUGGAGAAAGAAGAGAACUAGAAGACU UAAGAGAAAGAGACGGAAGGUGAGAGCCAGAUCCAAAUAAGCGGAUUAUGA GUAAAUAACUCUAAUUUUGUUUUAAAUUCUUUCAAGAGUAUCGUAAUGUCA UUGAUGAAUUAACAUGUUAGUUUCUAUUCUACCUCAUAAUGGAUCUAAAUU GCAUACUAAUCUCACGGUGGGGUGUAAACCAUUGCCUACUAUUUAUAUAGU GCUUUAUAUAUGUCUCACAUAGUUUAAUCAAUUGUCCGUUUUUUUGG
8	FJZ663	pBluescript II KS (+)	SalI-HF	GGAAAGAAUUGCCAUCUUGGCAAUUCAACAACAACAACAACAACAACAACAACAAC AACAACAACAACAACAACAACAACAACAAAAA**AUG**AGAGCCAAGUGGAGAAAGAA GAGAACUAGAAGACUUAAGAGAAAGAGACGGAAGGUGAGAGCCAGAUCCAA AUAAGCGGAUUAUGAGUAAAUAACUCUAAUUUUGUUUUAAAUUCUUUCAAG AGUAUCGUAAUGUCAUUGAUGAAUUAACAUGUUAGUUUCUAUUCUACCUCAU AAUGGAUCUAAAUUGCAUACUAAUCUCACGGUGGGGUGUAAACCAUUGCCU ACUAUUUAUAUAGUGCUUUAUAUAUGUCUCACAUAGUUUAAUCAAUUGUCCG UUUUUUUGG

RNA	Plasmid name	Cloning Vector	Digested for T7 Polymerase run-off transcription	Resulting RNA sequence (5'-3') made by T7 RNA Polymerase run-off transcription and purified by denaturing acrylamide gel electrophoresis
9	FJZ659	pBluescript II KS (+)	SalI-HF	GGAAACAACAACAACAACAACAACAACAACAACAACAACAACAACAAGAAUUGCCA UCUUGGCAAUUCCAACAACAACAACAACAAAAA**AUG**AGAGCCAAGUGGAGAAAGA AGAGAACUAGAAGACUUAAGAGAAAGAGACGGAAGGUGAGAGCCAGAUCCA AAUAAGCGGAUUAUGAGUAAAUAACUCUAAUUUUGUUUUAAAUUCUUUCAA GAGUAUCGUAAUGUCAUUGAUGAAUUAACAUGUUAGUUUCUAUUCUACCUC AUAAUGGAUCUAAAUUGCAUACUAAUCUCACGGUGGGGUGUAAACCAUUGC CUACUAUUUAUAUAGUGCUUUAUAUAUGUCUCACAUAGUUUAAUCAAUUGUC CGUUUUUUUGG
10	pSW104	pUC19	BamHI	GGAGACCACAUCGAUUCAAUCGAA**AUG**AGAGCCAAGUGGAGAAAGAAGAGA ACUAGAAGACUUAAGAGAAAGAGACGGAAGGUGAGAGCCAGAUCCAAAUAA GCGGAUUAUGAGUAAAUAACUCUAAUUUUGUUUUAAAUUCUUUCAAGAGUA UCGUAAUGUCAUUGAUGAAUUAACAUGUUAGUUUCUAUUCUACCUCAUAAUG GAUCUAAAUUGCAUACUAAUCUCACGGUGGGGUGUAAACCAUUGCCUACUAU UUAUAUAGUGCUUUAUAUAUGUCUCACAUAGUUUAAUCAAUUGUCCGUUUU UUUGG

Note: pUC plasmids do not have a T7 promoter, therefore it was included in the plasmid insert during cloning, 5' to the desired RNA sequence.

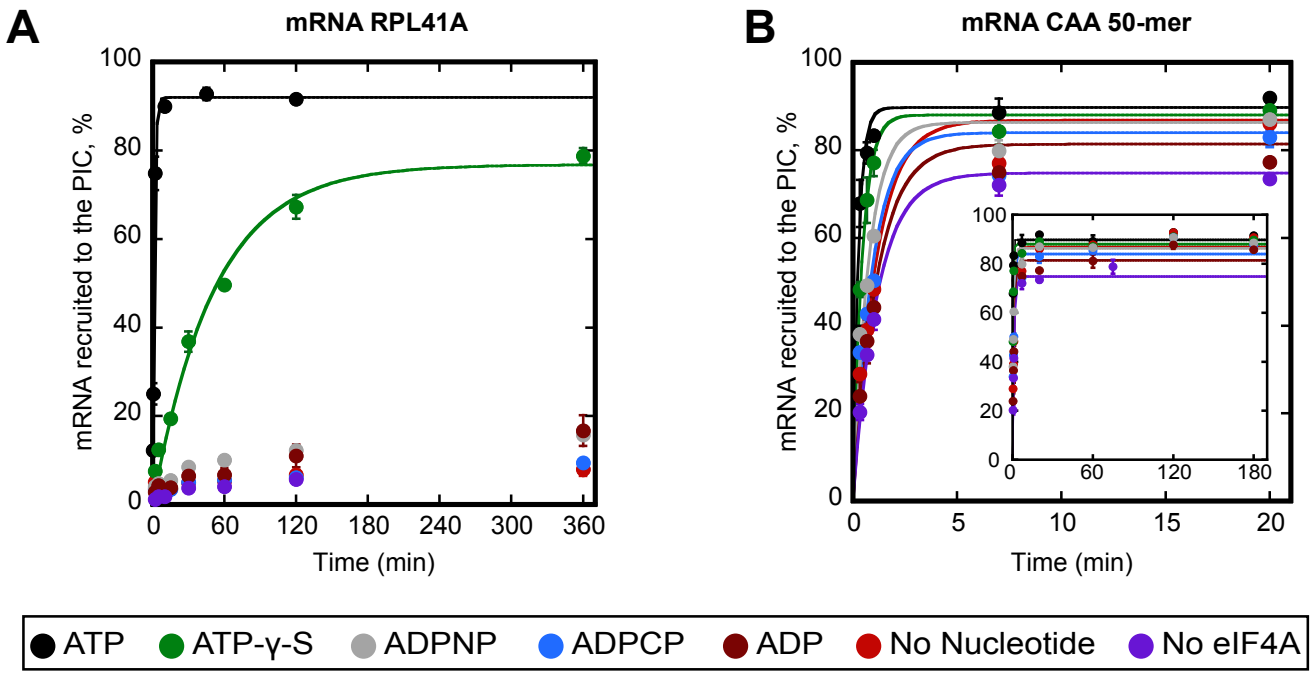

C

	RPL41A		CAA 50-mer	
	k_{obs} (min^{-1})	Endpoint (%)	k_{obs} (min^{-1})	Endpoint (%)
ATP	0.74 ± 0.01	92 ± 1	4.0 ± 0.6	90 ± 1
ATP-γ-S	0.019 ± 0.001	77 ± 2	2.3 ± 0.2	88 ± 1
ADPNP	ND	< 20	1.35 ± 0.02	86 ± 1
ADPCP	ND	< 10	1.08 ± 0.01	84 ± 1
ADP	ND	< 20	0.90 ± 0.1	81 ± 1
No Nucleotide	ND	< 10	0.90 ± 0.01	87 ± 1
No eIF4A	ND	< 10	0.90 ± 0.1	75 ± 1

Figure 1.

Figure 1. ATP hydrolysis by eIF4A stimulates recruitment of natural mRNA *RPL41A* as well as a synthetic 50-mer made up largely of CAA-repeats, presumed to be unstructured, with an AUG start codon 23 nucleotides from the 5'-end (CAA 50-mer). The concentration of ATP and analogs was 2 mM. **(A)** Percentage of *RPL41A* recruited to the PIC versus time. **(B)** Percentage of CAA 50-mer recruited to the PIC versus time. The larger plot shows the time-course up to 20 min. The inset is the entire time-course. **(C)** Observed rate constants (k_{obs}) and reaction endpoints from the data in panels A and B. All data in the figure are mean values ($n \geq 2$) and error bars represent average deviation of the mean. With *RPL41A*, rates with ADPNP, ADPCP, ADP, no nucleotide, and no eIF4A could not be measured accurately due to low endpoints ("ND").

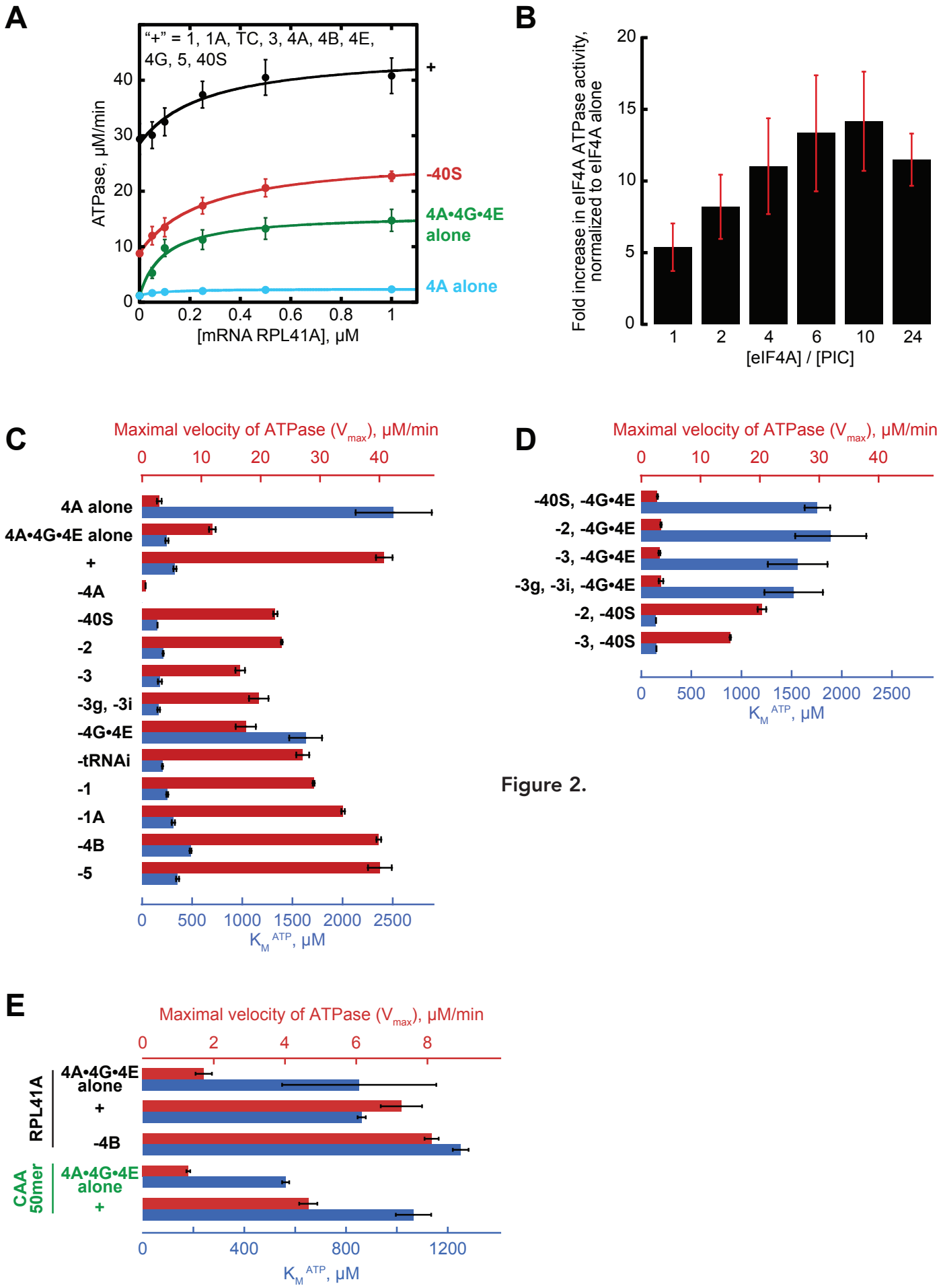
A
"+" = 1, 1A, TC, 3, 4A, 4B, 4E, 4G, 5, 40S
ATPase, μM/min
[mRNA RPL41A], μM
+
-40S
4A•4G•4E alone
4A alone
B
Fold increase in eIF4A ATPase activity, normalized to eIF4A alone
[eIF4A] / [PIC]
C
Maximal velocity of ATPase (V_{max}), μM/min
4A alone
4A•4G•4E alone
+
-4A
-40S
-2
-3
-3g, -3i
-4G•4E
-tRNAi
-1
-1A
-4B
-5
K_M^{ATP}, μM
D
Maximal velocity of ATPase (V_{max}), μM/min
-40S, -4G•4E
-2, -4G•4E
-3, -4G•4E
-3g, -3i, -4G•4E
-2, -40S
-3, -40S
K_M^{ATP}, μM
E
Maximal velocity of ATPase (V_{max}), μM/min
RPL41A
4A•4G•4E alone
+
-4B
CAA 50mer
4A•4G•4E alone
+
K_M^{ATP}, μM

Figure 2.

Figure 2. eIF4A and eIF4F ATPase activity is stimulated by the PIC. **(A)** ATPase activity in the presence of saturating ATP as a function of the concentration of capped *RPL41A* mRNA. "+" contains 5 μM eIF4A, 0.5 μM eIF4G•4E, 0.5 μM eIF4B, 0.5 μM eIF2, 0.5 μM Met-tRNA$_i$, 1 mM GDPNP•Mg^{2+}, 0.5 μM eIF3, 0.5 μM eIF5, 1 μM eIF1, 1 μM eIF1A, and 0.5 μM 40S subunits. Black: +, V_{max} = 45 ± 4 μM/min, K_m^{RNA} = 260 ± 40 μM. Red: -40S, V_{max} = 27 ± 1 μM/min, K_m^{RNA} = 270 ± 70 μM. Green: 5 μM eIF4A and 0.5 μM eIF4G•4E alone, V_{max} = 16 ± 1 μM/min, K_m^{RNA} = 100 ± 10 μM. Cyan: 5 μM eIF4A alone, V_{max} = 2.4 ± 0.2 μM/min, K_m^{RNA} = 80 ± 10 μM. **(B)** ATPase activity versus stoichiometry of eIF4A relative to the PIC, normalized to ATP hydrolysis with eIF4A alone. All reactions contained 5 mM ATP•Mg^{2+} and 0.5 μM capped *RPL41A* mRNA. All other concentrations are the same as in "+" in (A) except eIF4A, which are as indicated on the plot. **(C-D)** ATPase activity of eIF4A alone and in the context of eIF4G•4E, the PIC, or components of the PIC. “4A alone” was 5 μM eIF4A. “4A•4G•4E alone” was 5 μM eIF4A and 0.5 μM eIF4G•4E. "+" is the same as in (A). Components of the PIC that are missing with respect to "+" are indicated to the left of the bar graph. Red bars correspond to the top scale (red numbers), V_{max}; blue bars correspond to the bottom scale (blue numbers), K_m^{ATP}. **(E)** ATPase with 30 nM PIC. "+" contains 5 μM eIF4A, 0.05 μM eIF4G•4E, 0.3 μM eIF4B, 0.3 μM eIF2, 0.3 μM Met-tRNA$_i$, 0.5 mM GDPNP•Mg^{2+}, 0.3 μM eIF3, 0.3 μM eIF5, 1 μM eIF1, 1 μM eIF1A, 0.03 μM 40S, and 0.015 μM *RPL41A* (black) or CAA 50-mer (green). Red bars correspond to the top scale (red numbers), V_{max}; blue bars correspond to the bottom scale (blue numbers), K_m^{ATP}.

All data presented in the figure are mean values (n ≥ 2) and error bars represent average deviation of the mean.

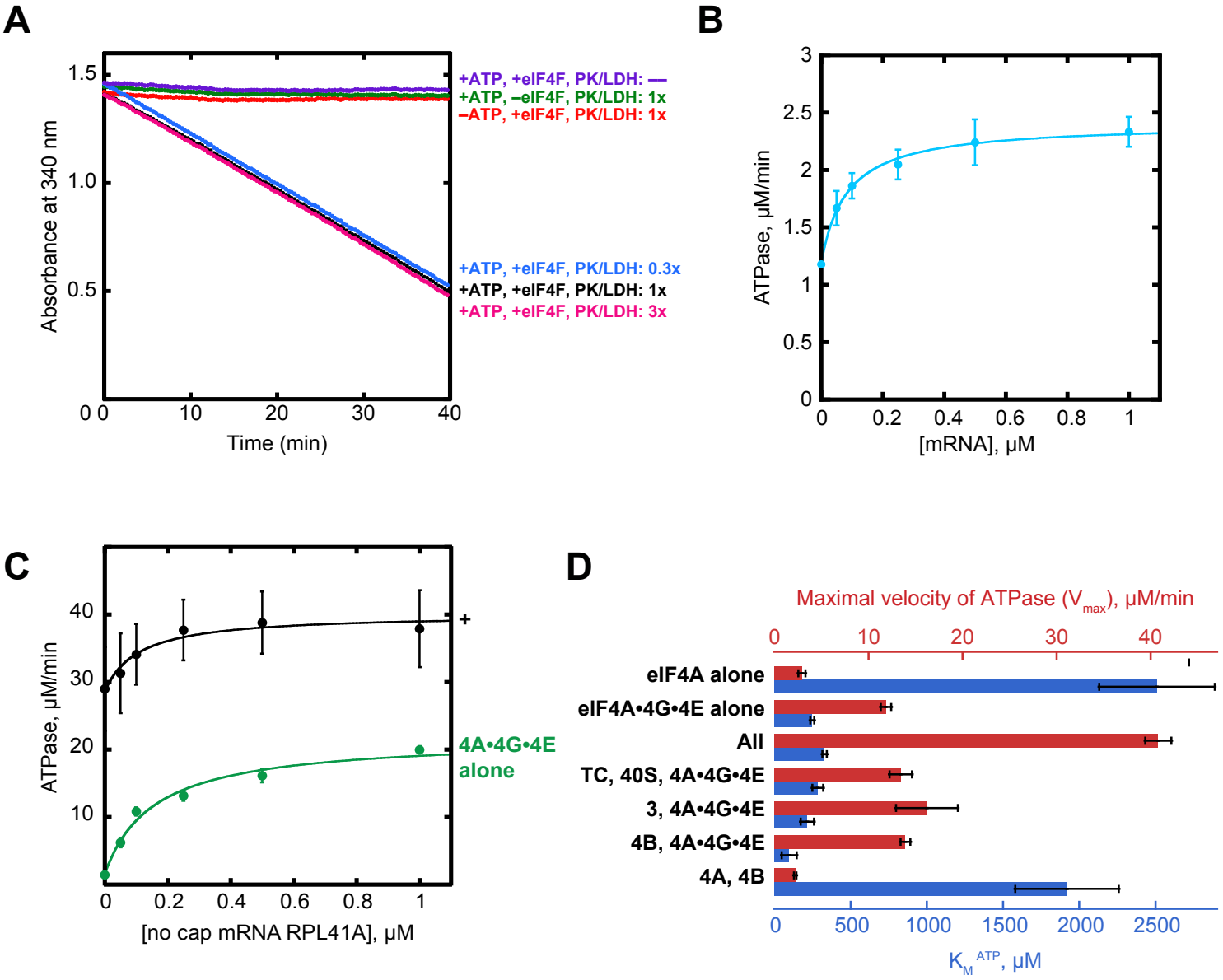

Figure 2 – Figure supplement 1.

Figure 2 – Figure supplement 1. Controls for eIF4A ATPase assays. **(A)** Controls for NADH enzyme-coupled microplate ATPase assay. The decrease in absorbance of 340 nm light was dependent on the presence of ATPase activity (5 μM eIF4A, 0.5 μM eIF4G•4E, together referred to as eIF4F), ATP, and a pyruvate kinase (900-1400 units/mL)/lactate dehydrogenase (600-1000 units/mL) mixture from rabbit muscle used as a 250x stock solution. **(B)** Capped *RPL41A* mRNA was titrated in the presence of 5 μM eIF4A and 5 mM ATP•Mg^{2+}. Data were fit with the Michaelis-Menten equation giving a V_{max} of 2.4 ± 0.2 μM/min and K_m^{RNA} of 80 ± 10 μM. **(C)** Uncapped *RPL41A* mRNA was titrated in the presence of 5 μM eIF4A and 0.5 μM eIF4G•4E alone (green) and had a V_{max} of 21.3 ± 0.1 μM/min and a K_m^{RNA} of 150 ± 20 μM or in the presence of the PIC ("+", black, same as in Figure 2A) and had a V_{max} of 40 ± 6 μM/min and a K_m^{RNA} of 120 ± 40 μM. **(D)** eIF4G•4E, eIF4B and eIF3, when present, were all 0.5 μM. "+" contained 5 μM eIF4A, 0.5 μM eIF4G•4E, 0.5 μM eIF4B, 0.5 μM eIF2, 0.5 μM Met-$tRNA_i$, 1 mM GDPNP•Mg^{2+}, 0.5 μM eIF3, 0.5 μM eIF5, 1 μM eIF1, 1 μM eIF1A, and 0.5 μM 40S subunits. "TC, 40S, 4A•4G•4E" contained 5 μM eIF4A, 0.5 μM eIF4G•4E, 0.5 μM 40S, 0.5 μM eIF2, 0.5 μM Met-$tRNA_i$, and 1 mM GDPNP•Mg^{2+}. Data in B-D are mean values (n ≥ 2) and error is reported as average deviation of the mean.

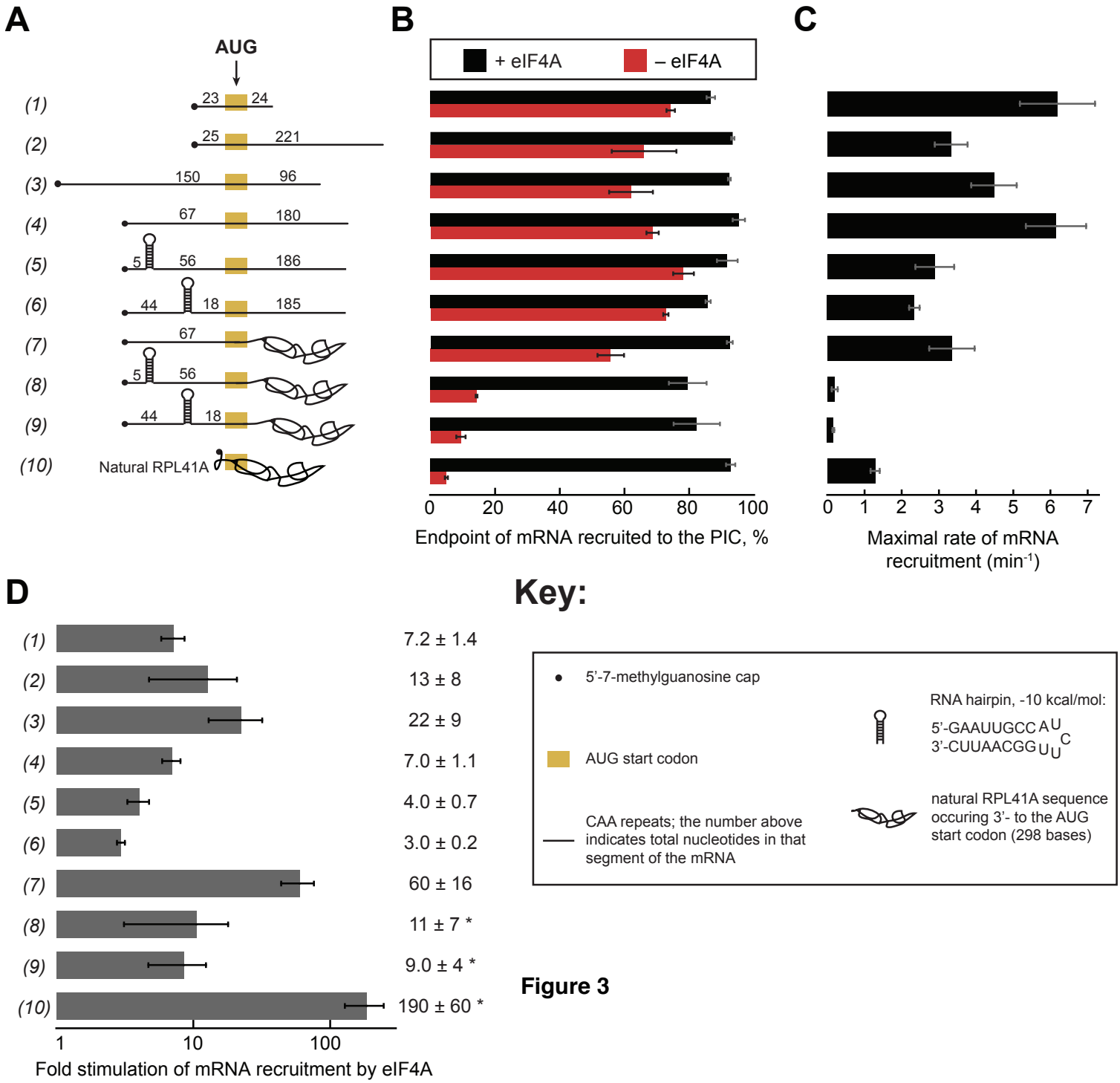
A
AUG
(1)
23
24
(2)
25
221
(3)
150
96
(4)
67
180
(5)
5
56
186
(6)
44
18
185
(7)
67
(8)
5
56
(9)
44
18
(10)
Natural RPL41A
B
+ eIF4A
– eIF4A
0
20
40
60
80
100
Endpoint of mRNA recruited to the PIC, %
C
0
1
2
3
4
5
6
7
Maximal rate of mRNA recruitment (min-1)
D
(1)
7.2 ± 1.4
(2)
13 ± 8
(3)
22 ± 9
(4)
7.0 ± 1.1
(5)
4.0 ± 0.7
(6)
3.0 ± 0.2
(7)
60 ± 16
(8)
11 ± 7 *
(9)
9.0 ± 4 *
(10)
190 ± 60 *
1
10
100
Fold stimulation of mRNA recruitment by eIF4A
Key:
5'-7-methylguanosine cap
AUG start codon
CAA repeats; the number above indicates total nucleotides in that segment of the mRNA
RNA hairpin, -10 kcal/mol:
5'-GAAUUGCC A U C
3'-CUUAACGG U U
natural RPL41A sequence occuring 3'- to the AUG start codon (298 bases)

Figure 3

Figure 3. eIF4A stimulates recruitment of mRNAs regardless of their degree of structure. **(A)** Schematic of mRNAs used in the study. mRNAs were capped unless otherwise noted but do not contain a poly(A) tail. Numbers on the mRNA indicate the total number of nucleotides in the corresponding segment of the RNA. **(B)** Endpoints of recruitment to the PIC for mRNAs in (A) in the presence (black) or absence (red) of saturating (5 μM) eIF4A. mRNAs are listed in the same order as in (A.) **(C)** Maximal rates of mRNA recruitment, k_{max} (min^{-1}), measured for the mRNAs in (A) (the corresponding time courses are shown in Figure 3 – figure supplement 1B-D) listed in the same order as in (A). **(D)** eIF4A-dependent stimulation of mRNA recruitment: the maximal rate of mRNA recruitment at saturating eIF4A concentration divided by the observed rate in the absence of eIF4A (calculated from data in Figure 3 – figure supplement 1E). Numbers to the left correspond to the mRNAs in (A). The asterisk (*) indicates that due to low recruitment endpoints in the absence of eIF4A, data for mRNAs 8 -10 could not be fit with an exponential rate equation and thus the fold stimulation by eIF4A was estimated from comparison of initial rates in the presence of saturating eIF4A versus the absence of eIF4A. All data presented in the figure are mean values ($n \geq 2$) and error bars represent average deviation of the mean.

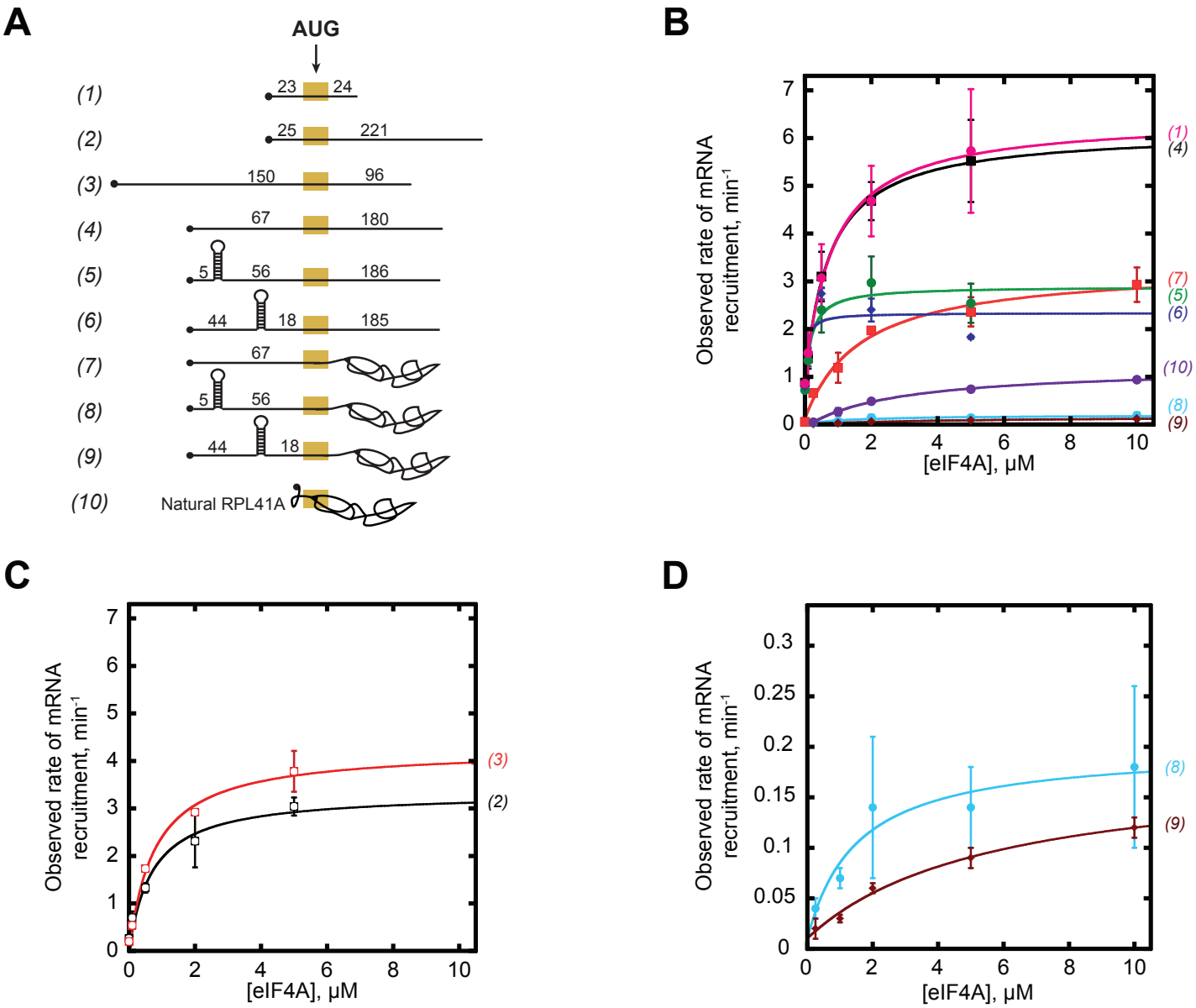

E

	$k_{obs}^{no\ eIF4A}$ (min^{-1})	k_{max} (min^{-1})	$K_{1/2}^{eIF4A}$ (μM)
(1)	0.90 ± 0.1	6.2 ± 1.0	0.70 ± 0.2
(2)	0.26 ± 0.16	3.3 ± 0.4	0.70 ± 0.03
(3)	0.20 ± 0.08	4.5 ± 0.6	1.0 ± 0.3
(4)	0.88 ± 0.07	6.2 ± 0.8	0.70 ± 0.01
(5)	0.72 ± 0.02	2.9 ± 0.5	0.20 ± 0.01
(6)	0.79 ± 0.02	2.3 ± 0.1	0.10 ± 0.02
(7)	0.06 ± 0.01	3.4 ± 0.6	1.8 ± 0.9
(8)	ND	0.20 ± 0.08	1.2 ± 0.2
(9)	ND	0.16 ± 0.02	3.5 ± 0.8
(10)	ND	1.3 ± 0.1	3.7 ± 1.0

Figure 3 – figure supplement 1.

Figure 3 – Figure supplement 1. eIF4A promotes recruitment of both structured and CAA-repeats mRNAs. **(A)** RNAs used in the study (same as (A) in Figure 3, shown again here for convenience). **(B-C)** Observed rates (k_{obs}) min^{-1} of mRNA recruitment as a function of the concentration of eIF4A. Data were fit with a hyperbolic equation allowing for a y-intercept > 0 (see Methods). Numbers in parentheses, to the right of the coordinate plane, correspond to mRNAs in (A) and are colored for easier visualization of distinct curves. RNAs 2 and 3 are shown separately for clarity. **(D)** Zoom of mRNAs 8 and 9 from (B) for clarity. **(E)** The observed rate of recruitment in the absence of eIF4A ($k_{obs}^{no\ eIF4A}$), the maximal rate of recruitment with saturating eIF4A (k_{max}), and the concentration of eIF4A required to achieve the half-maximal rate of recruitment ($K_{1/2}^{eIF4A}$) from fits in panels B-D. "ND:" the observed rate from an exponential fit could not be determined because of low reaction endpoint. All data presented in the figure are mean values (n ≥ 2) and error values are average deviation of the mean.

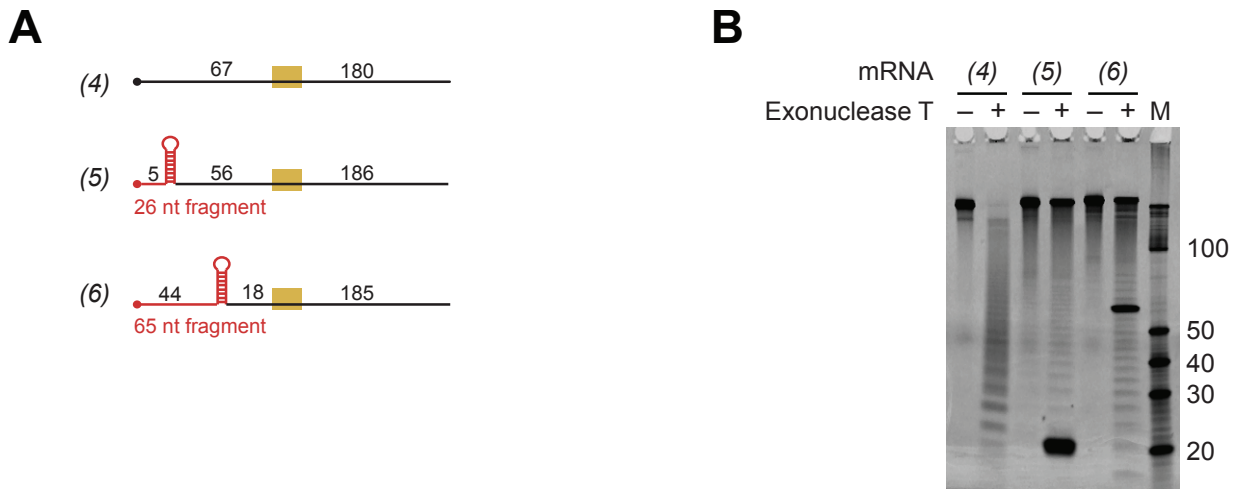

Figure 3 - figure supplement 2.

Figure 3 – Figure supplement 2. Evidence that the designed hairpins in the 5'-UTRs of mRNAs 4 and 5 are formed and that mRNA 4 lacks secondary structure. **(A)** RNAs 4-6 used in the study (same as in Figure 3A; shown again here for convenience). The fragments expected to be protected from 3'-5' RNase Exonuclease T digest are indicated in red. **(B)** RNAs 4-6 were incubated in the presence (+) or absence (–) of the 3'-5' RNase Exonuclease T, at the same temperature (26°C) used in all experiments in this study, for 18 hours. Reactions were resolved on a 15% Tris Borate EDTA Urea gel (4 pmol of total RNA per lane) and stained with SYBR Gold nucleic acid gel stain. “M:” Abnova Small RNA Marker. Marker RNA fragment sizes are indicated to the right of the gel.

Figure 4

A

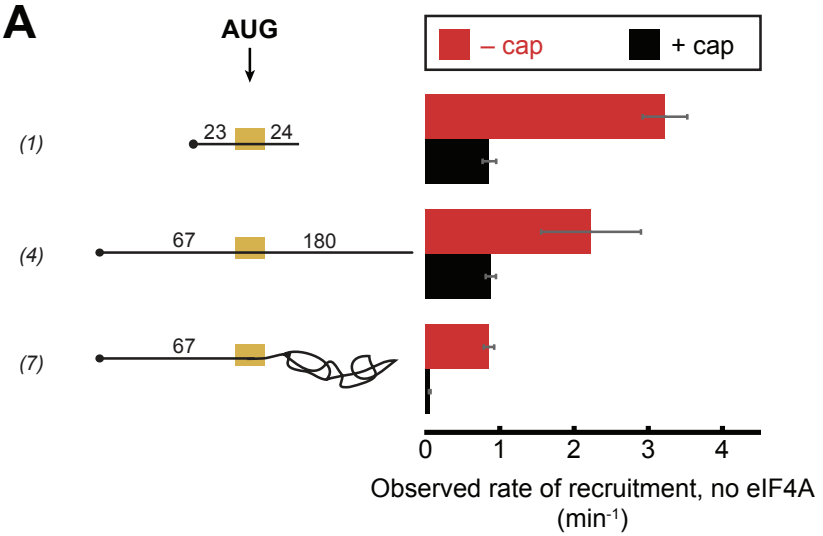

B

mRNA	5'-cap	$k_{obs}^{no\ eIF4A}$ (min^{-1})	k_{max} (min^{-1})	$\frac{k_{max}}{k_{obs}^{no\ eIF4A}}$	$\frac{k_{obs\ -cap}^{no\ eIF4A}}{k_{obs\ +cap}^{no\ eIF4A}}$
(1)	–	3.2 ± 0.3	4.3 ± 0.8	1.3 ± 0.3	**3.8 ± 0.5**
	+	0.9 ± 0.1	6.2 ± 1.0	7.2 ± 1.4	
(4)	–	2.2 ± 0.7	9.7 ± 0.7	4.4 ± 1.4	**2.5 ± 0.8**
	+	0.88 ± 0.07	6.2 ± 0.8	7.0 ± 1.1	
(7)	–	0.85 ± 0.07	4.0 ± 1.0	4.7 ± 1.2	**15 ± 3**
	+	0.06 ± 0.01	3.4 ± 0.6	60 ± 16	

Figure 4. The 5'-7-methylguanosine cap inhibits mRNA recruitment in the absence of eIF4A. Observed rates of mRNA recruitment (min^{-1}) when eIF4A was not included in the reaction, in the presence (black bars) or absence (red bars) of the 5'-cap. (See Figure 3A Key for explanation of mRNA diagrams). **(B)** The observed rates of recruitment in the absence of eIF4A ($k_{obs}^{no\ eIF4A}$), k_{max}, fold enhancement by eIF4A ($k_{max}/k_{obs}^{no\ eIF4A}$), and fold difference in the absence of eIF4A ($k_{obs\ -cap)}^{no\ eIF4A}$ / $k_{obs\ +cap}^{no\ eIF4A}$). The data for the capped mRNAs are reproduced from Figure 3 – figure supplement 1E for comparison purposes. “ND:” not determinable due to low reaction endpoint. All data presented in the figure are mean values (n ≥ 2) and error bars represent average deviation of the mean. Error was propagated when ratios were calculated.

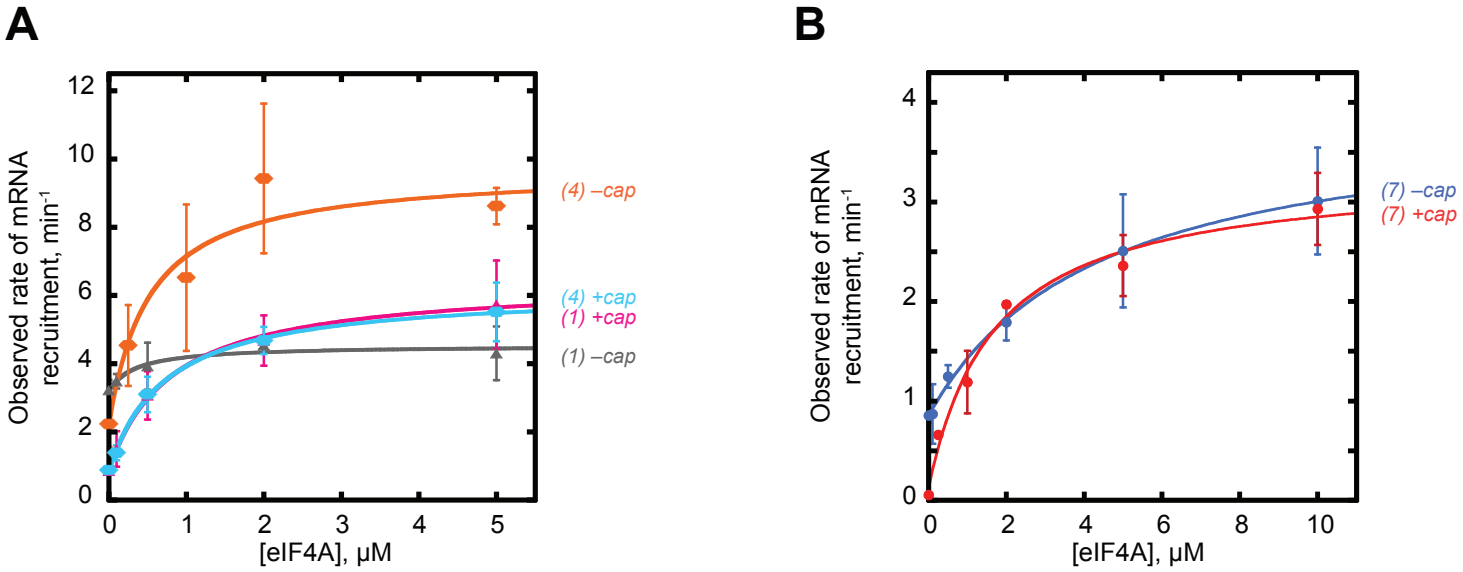

Figure 4 - Supplement 1.

Figure 4 – Figure supplement 1. The 5'-7-methylguanosine cap inhibits mRNA recruitment in the absence of eIF4A. **(A-B)** mRNA recruitment of (A) RNA 1 (CAA 50-mer), RNA 4, and (B) RNA 7 in the presence or absence of a 5'-cap, as indicated to the right of each curve. Numbers to the right of the plots correspond to RNAs in Figure 3A. All data presented in the figure are mean values ($n \geq 2$) and error bars represent average deviation of the mean.

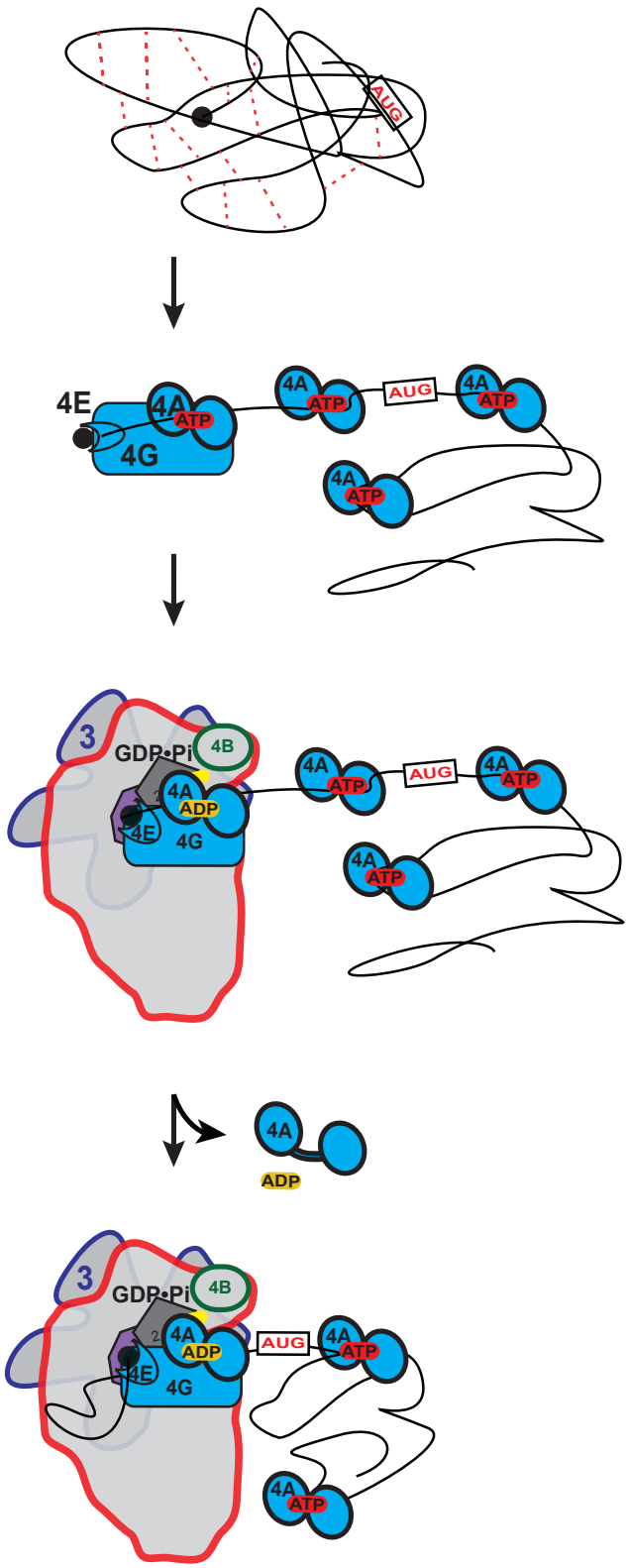
AUG
4E
4A
ATP
4G
4A
ATP
AUG
4A
ATP
4A
ATP
3
GDP•Pi
4B
4A
ADP
4E
4G
4A
ATP
AUG
4A
ATP
4A
ATP
4A
ADP
3
GDP•Pi
4B
4A
ADP
4E
4G
AUG
4A
ATP
4A
ATP

Figure 5.

Figure 5. A model for the mechanism of action of eIF4A in promoting mRNA recruitment to the PIC. mRNAs have complex, often dynamic, structures due to numerous local and distant interactions (red dotted lines) as well as the inherent tendency of polymers longer than their persistence lengths to fold back on themselves. These complex global structures can occlude the 5'-ends of the mRNAs and the start codon, making it difficult for the PIC to bind and locate them. eIF4F and individual eIF4A molecules keep the mRNA in a partially-unwound state until the PIC interacts with eIF4F, which stimulates the ATPase activity of the first eIF4A molecule. This eIF4A hydrolyzes ATP, threads or hands off the 5'-end of the mRNA into the entry channel of the 40S subunit, and dissociates from the complex. The next eIF4A on the 3' side of the PIC then binds to eIF4G and the cycle repeats, allowing the PIC to scan down the mRNA.